Depth-varying rupture properties of subduction zone megathrust faults

Thorne Lay,[1] Hiroo Kanamori,[2] Charles J. Ammon,[3] Keith D. Koper,[4] Alexander R. Hutko,[5] Lingling Ye,[1] Han Yue,[1] and Teresa M. Rushing[1]

Received 3 January 2012; revised 6 March 2012; accepted 10 March 2012; published 21 April 2012.

[1] Subduction zone plate boundary megathrust faults accommodate relative plate motions with spatially varying sliding behavior. The 2004 Sumatra-Andaman (M_w 9.2), 2010 Chile (M_w 8.8), and 2011 Tohoku (M_w 9.0) great earthquakes had similar depth variations in seismic wave radiation across their wide rupture zones – coherent teleseismic short-period radiation preferentially emanated from the deeper portion of the megathrusts whereas the largest fault displacements occurred at shallower depths but produced relatively little coherent short-period radiation. We represent these and other depth-varying seismic characteristics with four distinct failure domains extending along the megathrust from the trench to the downdip edge of the seismogenic zone. We designate the portion of the megathrust less than 15 km below the ocean surface as domain A, the region of tsunami earthquakes. From 15 to ~35 km deep, large earthquake displacements occur over large-scale regions with only modest coherent short-period radiation, in what we designate as domain B. Rupture of smaller isolated megathrust patches dominate in domain C, which extends from ~35 to 55 km deep. These isolated patches produce bursts of coherent short-period energy both in great ruptures and in smaller, sometimes repeating, moderate-size events. For the 2011 Tohoku earthquake, the sites of coherent teleseismic short-period radiation are close to areas where local strong ground motions originated. Domain D, found at depths of 30–45 km in subduction zones where relatively young oceanic lithosphere is being underthrust with shallow plate dip, is represented by the occurrence of low-frequency earthquakes, seismic tremor, and slow slip events in a transition zone to stable sliding or ductile flow below the seismogenic zone.

Citation: Lay, T., H. Kanamori, C. J. Ammon, K. D. Koper, A. R. Hutko, L. Ye, H. Yue, and T. M. Rushing (2012), Depth-varying rupture properties of subduction zone megathrust faults, *J. Geophys. Res.*, *117*, B04311, doi:10.1029/2011JB009133.

1. Introduction

[2] Large variations in pressure, temperature, pore fluids, sediment properties, fault roughness and geometry, fault zone maturity, mineral phase, and rock type are expected along the seismogenic portion of subduction zone megathrust faults [e.g., *Byrne et al.*, 1988; *Hyndman and Wang*, 1993; *Hyndman et al.*, 1995; *Dixon and Moore*, 2007; *Lay and Bilek*, 2007; *Heuret et al.*, 2011]. As frictional sliding behavior is plausibly influenced by all of these fault zone properties, observations of depth-varying earthquake phenomena along the megathrust are not surprising [*Marone and Scholz*, 1988; *Scholz*, 1998; *Bilek*, 2007; *Wang and He*, 2008]; however, systematic variations with depth have been difficult to resolve because along-strike variations tend to be as strong or stronger in many regions [e.g., *Yomogida et al.*, 2011], and up until the last decade seismic observations were too limited to resolve any depth-varying frequency-dependence in very large ruptures.

[3] Perhaps the best-established attribute of depth-varying properties of megathrust earthquakes is the distinct behavior of the upper 5 to 10 km of the fault zone commonly overlain by an accretionary prism. This region is generally thought to accommodate relative plate motions aseismically, with near-trench sediments undergoing significant anelastic deformation, velocity-strengthening frictional properties of the megathrust inhibiting nucleation of earthquake instabilities, and overall low seismicity levels. However, intermittent large-slip

[1]Department of Earth and Planetary Sciences, University of California, Santa Cruz, California, USA.
[2]Seismological Laboratory, California Institute of Technology, Pasadena, California, USA.
[3]Department of Geosciences, Pennsylvania State University, University Park, Pennsylvania, USA.
[4]Department of Geology and Geophysics, University of Utah, Salt Lake City, Utah, USA.
[5]Incorporated Research Institutions for Seismology Data Management Center, Seattle, Washington, USA.

0148-0227/12/2011JB009133

ruptures of this shallow region do occur, establishing the potential for tsunamigenic seismic failure of the megathrust all the way to the trench in at least some, and possibly many, regions.

[4] The central portion of the megathrust is where most large interplate ruptures occur, and much focus has been placed on understanding regional variations in the maximum size and rupture complexity of 'typical' megathrust failures [e.g., *Kanamori*, 1986; *Kikuchi and Fukao*, 1987; *Thatcher*, 1989]. Depth-dependent variations in rupture process across this central portion of the megathrust have been noted previously, but only recently demonstrated to be significant for great earthquake ruptures. Further downdip, the megathrust transitions to aseismic fault displacement, and for subduction zones like Southwest Japan and Cascadia the transition appears to involve a zone with a mix of episodic slow slip, low frequency earthquakes, and seismic tremor comprised of many small earthquakes cascading in prolonged sequences [e.g., *Peng and Gomberg*, 2010; *Beroza and Ide*, 2011; *Ide*, 2012; *Vidale and Houston*, 2012].

[5] In this study, we extend the general characterization of depth-varying megathrust behavior described above to include a subdivision of the central portion of megathrusts, motivated by distinctions in the seismic radiation spectra of great and moderate size events as a function of depth. This leads to a four-domain characterization of earthquake rupture properties along-dip on megathrusts. Strong lateral variations exist in all four domains; however, our conceptual model provides a framework for characterizing and comparing earthquakes and frictional regimes in different subduction zones that incorporates a broad suite of observations of earthquakes and that can guide quantitative studies of the myriad local influences on rupture processes.

2. The Accretionary Toe Portion of the Megathrust

[6] The shallowest megathrust region, where confining pressures are low and pore fluids and unconsolidated sediments are most likely to exist in the fault zone, tends to have either anelastic deformation and aseismic stable or episodic sliding [e.g., *Byrne et al.*, 1988; *Moore and Saffer*, 2001; *Wang and Hu*, 2006; *Hu and Wang*, 2008], or to fail seismically in a special class of events called tsunami earthquakes [*Kanamori*, 1972; *Newman and Okal*, 1998; *Polet and Kanamori*, 2000; *Lay and Bilek*, 2007]. The existence of a 'seismic backstop', or seaward limit to the occurrence of small seismic activity, and evidence for anelastic deformation of sediments near the toe of accretionary prisms, suggest that velocity-strengthening friction likely dominates at very shallow depth. This is often invoked as an argument that seismic failure is unlikely, but this may under-represent the seismogenic potential of the shallowest part of the plate boundary in many regions.

[7] Moderate size earthquakes ($M_w \sim 6$ to 7) that do occur in the shallowest ~40 km wide portion of the megathrust (5–15 km below the ocean surface) can have anomalously long source time function durations, possibly indicating widespread presence of low-rigidity material in the fault zone [*Bilek and Lay*, 1999; *Lay and Bilek*, 2007]. While the megathrust may be velocity-strengthening in the toe region, if rupture nucleates at somewhat greater depth along the megathrust it may propagate all the way to the trench as a result of conditional stability of fault friction [e.g., *Scholz*, 1998; *Hu and Wang*, 2008]. Thus the seismic backstop may define the updip rupture extent for small ruptures, but large tsunami earthquake ruptures may extend further updip.

[8] Tsunami earthquakes usually involve large megathrust slip and seafloor motion near the sedimentary wedge toe of the overriding plate, which generates large displacement of the overlying water. These ruptures have been found to have anomalously weak short-period seismic radiation, yielding low m_b (~1 s period) and M_S (~20 s period) seismic magnitudes relative to long-period source strength [*Kanamori*, 1972]. Tsunami earthquakes have been documented in Japan (1896), Alaska (1946), Kuril Islands (1963, 1975), Nicaragua (1992), Peru (1960, 1996), Java (1994, 2006), and Indonesia (1907, 2010). Well-studied recent tsunami earthquakes have unusually long rupture processes, similar to unusually long-duration moderate size events at shallow depths [*Bilek and Lay*, 2002], low seismic moment-scaled energy release, and low rupture velocities, probably related to low source region rigidity (and accompanying low shear velocity), which is also associated with the occurrence of relatively large slip for a given seismic moment [*Kanamori and Kikuchi*, 1993; *Velasco et al.*, 1994; *Satake*, 1994; *Ammon et al.*, 2006; *Lay and Bilek*, 2007; *Lay et al.*, 2011b; *Newman et al.*, 2011]. The large slips involved make it likely that these events displace the fault all the way to the trench, although some tsunami earthquakes may rupture splay or backstop frontal faults in addition to the main megathrust [e.g., *Fukao*, 1979; *Moore et al.*, 2007; *Singh et al.*, 2011].

[9] Tsunami earthquakes have been located both in regions where the deeper megathrust has not been observed to have great thrust events (e.g., Java, Peru, and Japan), and in regions where great thrust events do occur downdip (e.g., Kuril Islands, Indonesia). The latter situation is of particular importance given that the majority of great underthrusting earthquakes do not appear to involve coseismic rupture extending all the way to the trench (the 2011 Tohoku event is a rare well-documented exception). The 25 October 2010 Mentawai (M_w 7.8) tsunami earthquake [*Lay et al.*, 2011b; *Newman et al.*, 2011] ruptured at very shallow depth updip of the deeper megathrust rupture on 12 September 2007 (M_w 7.9), and the 1907 Sumatra tsunami earthquake [*Kanamori et al.*, 2010] appears to have ruptured updip of the region that later failed in the great 2005 (M_w 8.6) underthrusting event. The 2010 Mentawai event appears to have nucleated at about 10 km depth, with rupture propagating up to the trench, so it may be an instance of deeper nucleation driving failure of shallow conditionally stable material. One thus cannot have high confidence that regions updip of large megathrust events will not have tsunami earthquakes unless the absence of shallow megathrust strain accumulation can be independently established. Of course some regions may be undergoing stable sliding or have slow-slip events (and seismic tremor), preventing large strain accumulation, so tsunami earthquakes may not occur everywhere. However, if there is a shallow frictional environment of conditional stability, rupture that nucleates at greater depth may drive faulting

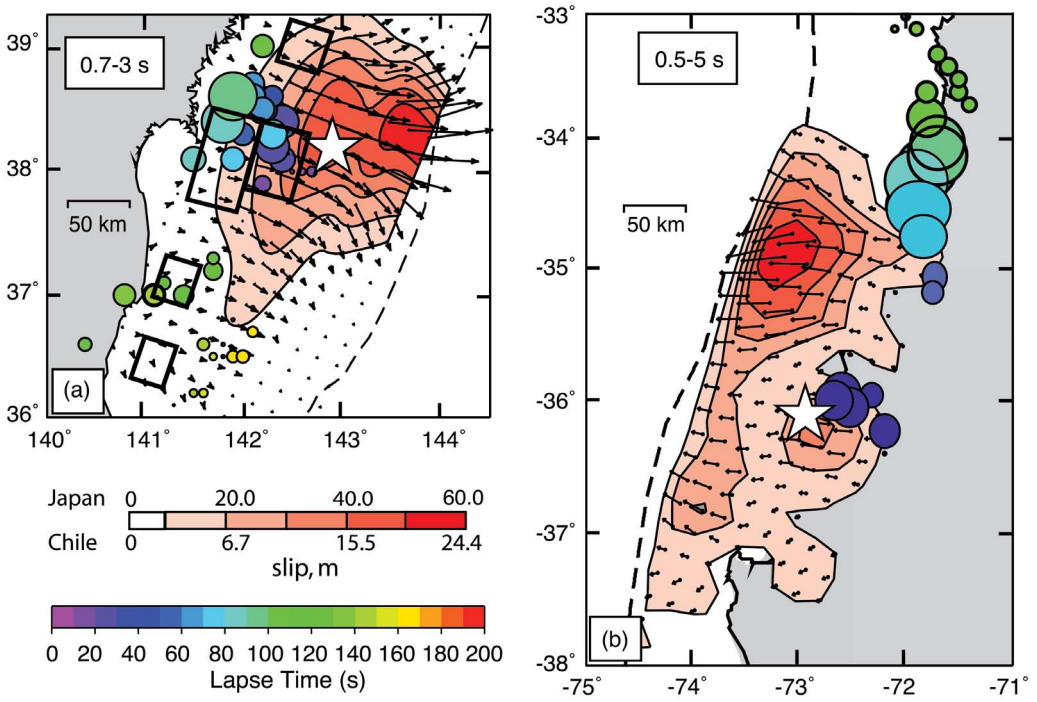

Figure 1. Maps summarizing rupture characteristics for (a) the 11 March 2011 Tohoku, Japan (M_w 9.0) and (b) the 27 February 2010 Maule, Chile (M_w 8.8) earthquakes. The white stars indicate the epicentral locations used for each rupture model. The coseismic slip distributions are those determined from high-rate GPS recordings for the Tohoku event by *Yue and Lay* [2011] and for the Chile event by *Koper et al.* [2012]. The vectors indicate the variable slip direction for subfaults, with the contoured color scale indicating the total slip at each position. The position and timing of sources of coherent short-period teleseismic P wave radiation in the bandpass indicated in each panel imaged by back-projection of recordings at North American seismic stations, mainly from the EarthScope Transportable Array, are shown by the colored circles, with radius scaled proportional to relative beam power (from *Koper et al.* [2011b] for Tohoku, and *Koper et al.* [2012] for Chile). The rectangles in Figure 1a indicate estimated source locations of high frequency strong ground motions determined by *Kurahashi and Irikura* [2011]. Note that the regions with large slip locate updip, toward the trench (dashed line) in each case, whereas the coherent short-period radiation is from downdip, near the coastline.

of the shallow toe [e.g., *Hu and Wang*, 2008] with attendant strong tsunami excitation.

3. Great Earthquake Ruptures Across Megathrusts

[10] Most large subduction zone underthrusting earthquakes rupture within the 60 to 160 km wide portion of the megathrust extending from depths below sea level of about 15 km to 45–55 km. Earthquakes in this depth range vary greatly in complexity and slip distribution, but have hitherto been viewed as basically similar in seismic radiation as a function of depth along the megathrust. However, the recent occurrence of great earthquakes with very wide along-dip rupture extent, and the availability of extensive seismic wave recordings that allow detailed analysis, indicate that there are systematic differences in seismic radiation as a function of depth on this central portion of the megathrust.

[11] The clearest evidence for this is provided by the 27 February 2010 Chile (M_w 8.8, m_b 7.2) and 11 March 2011 Tohoku (M_w 9.0, m_b 7.2) great earthquakes. For both events, seismic observations clearly indicate depth-variations in frequency dependent seismic radiation (Figure 1). Sources of coherent short-period (~1 s) radiation are imaged in the downdip portions of the megathrusts by large seismic network back-projection methods for the Chile [*Lay et al.*, 2010b; *Kiser and Ishii*, 2011; *Koper et al.*, 2012; *Wang and Mori*, 2011b] and Tohoku [*Koper et al.*, 2011a, 2011b; *Ishii*, 2011; *Wang and Mori*, 2011a; *Meng et al.*, 2011; *Yao et al.*, 2011; *Zhang et al.*, 2011] events. For the 2011 Tohoku earthquake the locations of sources of teleseismic short-period radiation plot close (Figure 1) to locations of strong ground motion accelerations determined by *Kurahashi and Irikura* [2011], suggesting a common origin. Inversions and modeling of seismic, geodetic, and tsunami observations indicate large slip updip of the short-period sources for the Chile [e.g., *Lay et al.*, 2010b; *Delouis et al.*, 2010; *Tong et al.*, 2010; *Lorito et al.*, 2011; *Pollitz et al.*, 2011b; *Vigny et al.*, 2011] and Tohoku [e.g., *Ammon et al.*, 2011; *Fujii et al.*, 2011; *Hayes*, 2011; *Ide et al.*, 2011; *Iinuma et al.*, 2011; *Koketsu et al.*, 2011; *Lay et al.*, 2011a, 2011c; *Maeda et al.*, 2011; *Ozawa et al.*,

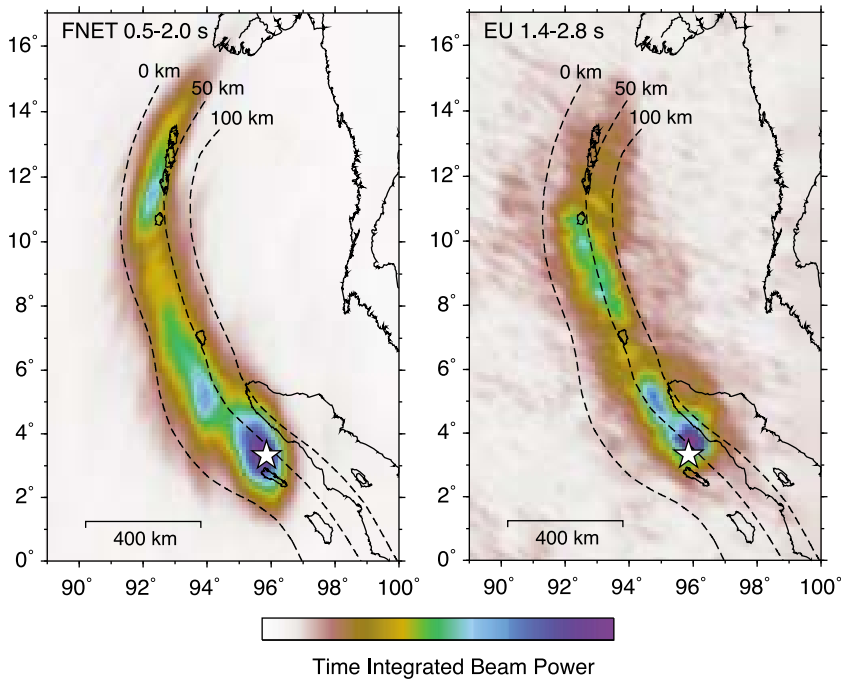

Figure 2. Maps of the time-integrated back-projected teleseismic P wave beams at each grid point in the source region of the 26 December 2004 Sumatra earthquake for data from (left) F-net stations in Japan and (right) broadband stations in Europe; dominant period ranges are indicated in each panel. The USGS epicenter is indicated by the white stars. Dashed contour lines indicate the trench (left-most contours), and slab depths of 50 km and 100 km as defined by the approximate top of the seismogenic zone [*Gudmundsson and Sambridge*, 1998]. Both images show that coherent short-period energy was radiated well downdip of the trench.

2011; *Pollitz et al.*, 2011a; *Shao et al.*, 2011; *Simons et al.*, 2011; *Yoshida et al.*, 2011; *Yue and Lay*, 2011] events, as illustrated in Figure 1.

[12] There is a tendency for inversions of GPS static ground motions for the 2011 Tohoku event to place large slip primarily near the center of the megathrust, while seismic and tsunami inversions indicate 50–80 m displacements near the toe. Inversions of high-rate GPS recordings [*Yue and Lay*, 2011] place concentrations of slip both near the hypocenter and near the trench (Figure 1), indicating that time-dependence of the near-field ground motions may resolve the discrepancy. The shallowest portion of the 2011 Tohoku rupture appears to have behaved like a tsunami earthquake. It is not yet resolved whether the 2010 Chile event ruptured to the trench; our modeling of tsunami observations using seismic wave inversion models [*Lay et al.*, 2010b] favors slip being relatively far offshore, but not peaking near the trench as for the 2011 Tohoku rupture. Recent geodetic inversions also place slip further offshore than earlier models for the 2010 Chile event, although again not extending all the way to the trench [e.g., *Vigny et al.*, 2011].

[13] The great 2004 Sumatra-Andaman (M_w 9.2, m_b 6.8) earthquake ruptured over 1300 km along strike, with faulting extending from the broad megathrust region along northern Sumatra to the narrower subduction zones along the Nicobar and Andaman Islands. We focus our attention on the megathrust region along Sumatra, where the largest slip and widest fault are found. The seismic and geodetic observations for this rupture generally agree in placement of large slip west of northernmost Sumatra [e.g., *Ammon et al.*, 2005; *Vigny et al.*, 2005; *Chlieh et al.*, 2007; *Rhie et al.*, 2007], although there are significant variations in model parameterization and placement of slip along dip [*Poisson et al.*, 2011]. We favor the models that provide good fit to the tsunami observations, as along-dip resolution is limited for both seismic and geodetic inversions. *Fujii and Satake* [2007] and *Poisson et al.* [2011] show that models with slip extending significantly offshore, like that from joint seismic and geodetic inversion by *Rhie et al.* [2007], fit the timing of deep water tsunami observations particularly well. Aftershocks also appear to extend to close to the trench, suggesting at least some very shallow displacement on the megathrust.

[14] The observations of depth-varying seismic radiation for the 2010 Chile and 2011 Tohoku events motivated us to revisit back-projections of short-period signals, which were originally performed soon after the 2004 Sumatra-Andaman rupture [*Ishii et al.*, 2005, 2007; *Krüger and Ohrnberger*, 2005a, 2005b]. These earlier studies emphasized the general correspondence of along-strike patterns in coseismic slip and short-period radiation, but they do differ in along-dip placement of the sources of coherent teleseismic short-period radiation, with imaging using European networks favoring more downdip locations than imaging using stations in Japan.

[15] We perform new back-projections using two large-scale networks of seismic stations using the method of *Xu et al.* [2009] to determine the locations of coherent

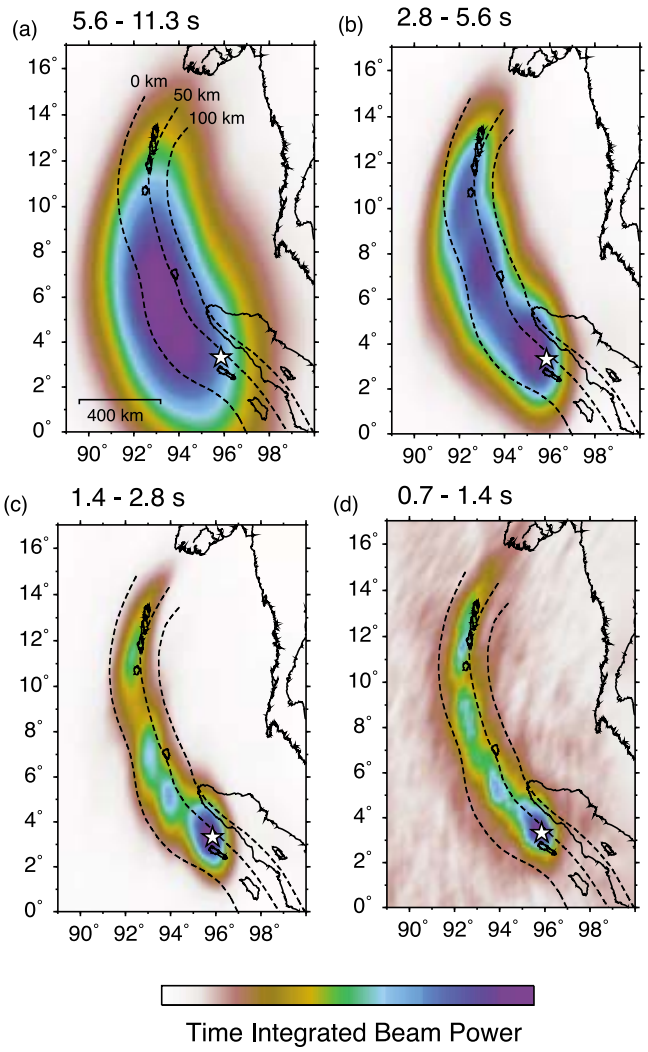

Figure 3. Time-integrated maps of the back-projected teleseismic P wave beams at each grid point in the source region of the 26 December 2004 Sumatra earthquake for F-net data narrowly band-pass filtered around periods (a) 8 s, (b) 4 s, (c) 2 s, and (d) 1 s. The USGS epicenter is indicated by the white star. Dashed contour lines indicate the trench (left-most contours), and slab depths of 50 km and 100 km as defined by the approximate top of the seismogenic zone. The 8-s period range image shows energy closer to the trench than the three shorter-period images, and is more similar to slip models derived from waveform inversion.

teleseismic short-period radiation from the 2004 Sumatra-Andaman rupture. Recordings from 70 stations of the F-net broadband network in Japan and 57 broadband stations in Europe were selected for relatively uniform spatial distribution and high data quality, aligned by multistation cross-correlation [*VanDecar and Crosson*, 1990], and narrowband filtered with central periods of 1 s and 2 s, respectively. The travel times from each node in a source-region imaging grid to each station were computed for the reference model AK135 [*Kennett et al.*, 1995]. The data traces aligned on the early portion of the signal were then shifted for predicted relative move out from each grid point and summed with fourth-root stacking; forming a two-dimensional spatial grid of time-varying data beam power. The time-varying images formed from the F-net and European data are shown in Movie S1 of the auxiliary material, and time-integrated images of the data beams at each grid point are shown in Figure 2.[1] The images from the European data are compatible with prior work [*Krüger and Ohrnberger*, 2005a, 2005b], and are quite similar to our images from F-net data, allowing for differences in directivity and intrinsic sensitivity of the two network configurations. There are some differences in along-strike placement of short-period energy sources for the two networks, which may be partly the result of small differences in passband but is most likely due to azimuthal variation in the Green functions and relative importance of depth phases versus direct phases at varying azimuths [e.g., *Lay et al.*, 2010c] combined with network response effects. There is still minor discrepancy in along-dip placement of the short-period sources between the two network images, but in both cases the radiation is imaged as originating from relatively close to the coastline.

[16] Figure 3 is a complementary display of the frequency dependence within the short-period passband, showing time-integrated beam power maps from fourth-root back-projection of F-net data in four narrow, overlapping passbands centered at 8 s, 4 s, 2 s, and 1s. The three shorter-period images consistently indicate a predominantly downdip pattern of energy release along northern Sumatra, while the longer period image indicates source energy radiating from shallower on the broad megathrust, more consistent with slip models derived from waveform inversion of seismic and geodetic data. Imaging with longer period signals than these has insufficient spatial resolution to detect any depth-dependence.

[17] To evaluate whether there is any bias in the back-projection of the short-period energy to the source region, extended duration seismograms were processed for the same station configurations and images were formed for time intervals spanning large early aftershocks along the megathrust. The apparent locations of coherent short-period energy formed from the F-net beams in the passband centered at 1 s are close to the USGS National Earthquake Information Center (NEIC) source locations (Figure 4), indicating that there is no major systematic bias in the back-projection of short-period signal energy over the southern portion of the 2004 rupture zone. The megathrust dip appears to increase in the region of the short-period source locations [*Banerjee et al.*, 2007], but the teleseismic back-projections have no relative depth resolution.

[18] These new back-projections for the 2004 Sumatra-Andaman event resemble those for the 2010 Chile and 2011 Tohoku events in that they indicate concentration of the coherent short-period energy sources in the downdip portion of the megathrust. While the precise placement of coseismic slip for the 2004 event is not uniquely resolved, there still appear to be systematic differences in the locations of large slip and the short-period energy sources, similar to the more recent events. Schematic characterizations of the rupture attributes of all three events are shown in Figure 5. While there are some along-strike separations in regions of large

[1] Auxiliary materials are available in the HTML. doi:10.1029/2011JB009133.

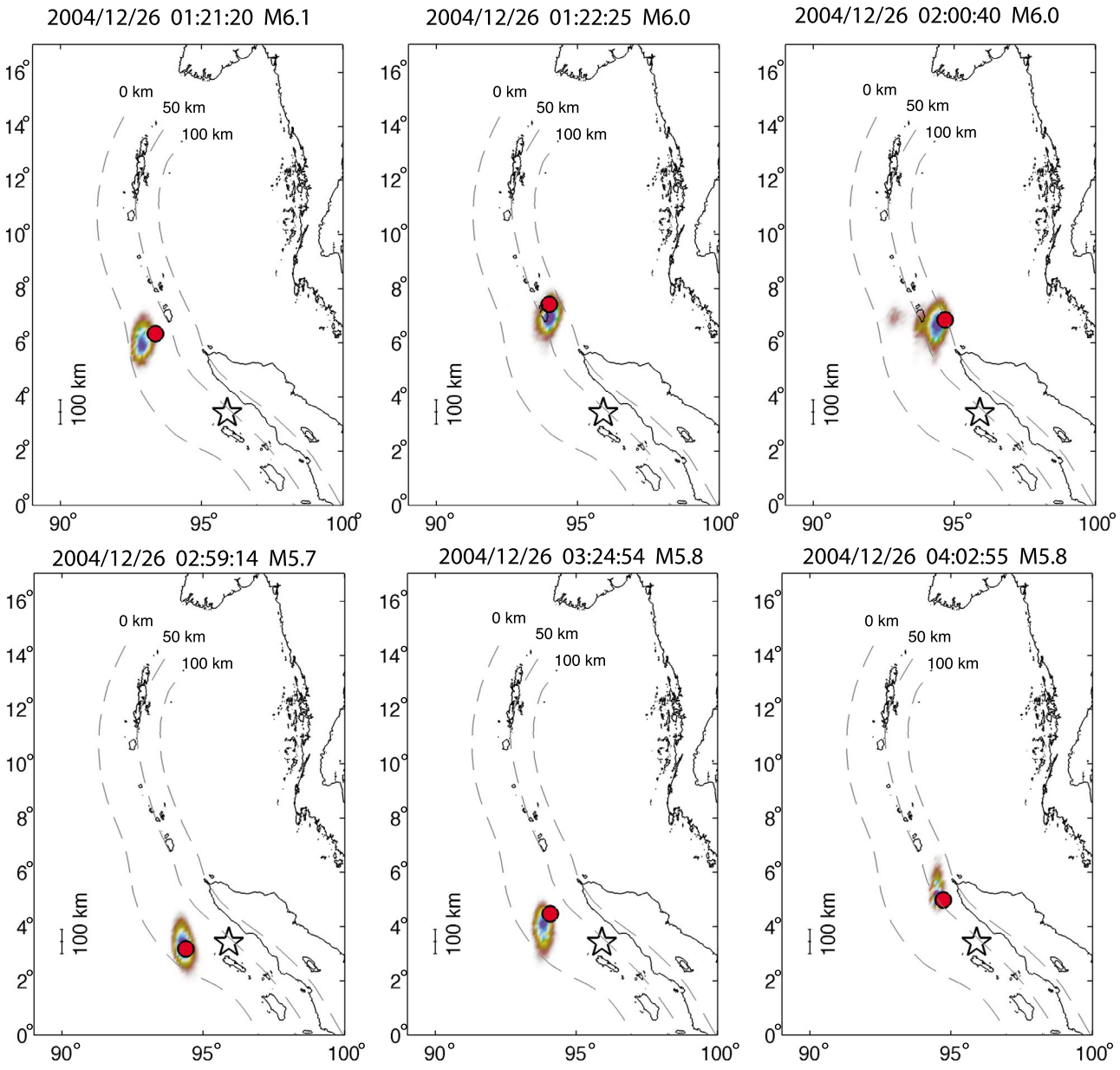

Figure 4. Comparison of large aftershock locations for the 26 December 2004 Sumatra Earthquake (NEIC epicenters are given by purple dots) and teleseismic P wave fourth-root stack back-projections of F-net data filtered around 1 s. The back-projections image short-period source radiation close to the NEIC locations, indicating that there is no systematic bias that would cause short-period images to form downdip of true source locations for the paths to F-net.

slip and short-period radiation, the evidence for systematic depth-variation is strong.

4. Deep Megathrust Transition to Aseismic Motion

[19] All megathrust faults have downdip limits to their seismogenic zones, below which only aseismic sliding or plastic deformation accommodates plate convergence. For many regions seismic activity indicates that this transition is relatively abrupt at depths of 45–55 km [e.g., *Tichelaar and Ruff*, 1993], but there may be a deeper extent of conditionally stable state that allows rupture to extend downdip during very large events. Recent observations have established that there can be a transitional region in which a mix of slow slip events, low frequency events, and seismic tremor phenomena occur. This has been documented to occur at depth of 30–45 km in several subduction zones, typically involving subduction of relatively young plates with shallow dip angles (Southwest Japan, Cascadia, Central America) (see reviews by *Beroza and Ide* [2011] and *Ide* [2012]). This transitional behavior is not clearly manifested everywhere; for example, no tremor or slow-slip events have been reported downdip of the 2011 Tohoku rupture zone despite extensive instrumentation. At this time, it appears that the transition from seismogenic to aseismic sliding can be

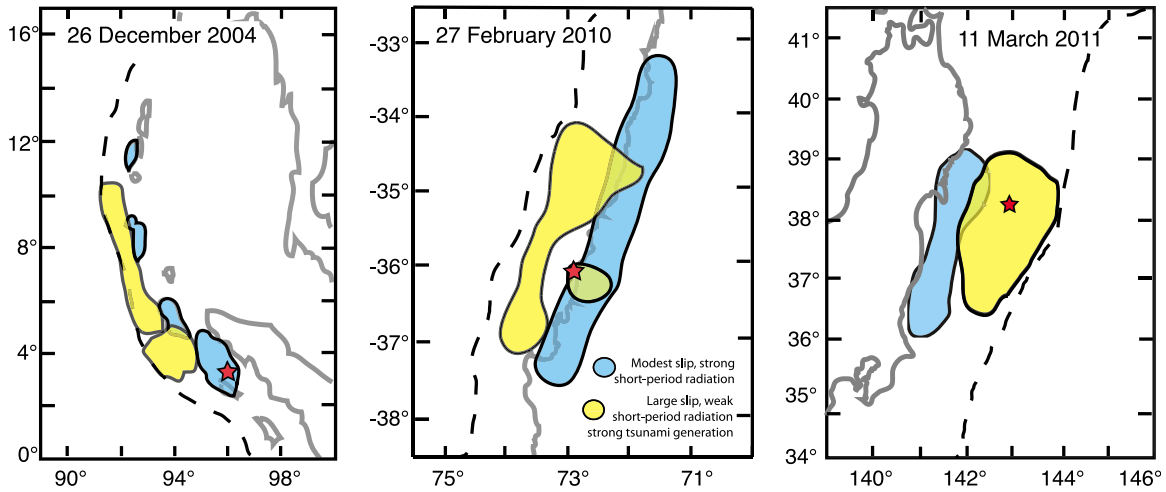

Figure 5. Schematic summary of patterns of coherent short-period radiation and large coseismic slip regions for the great (left) 26 December 2004 Sumatra (M_w 9.2), (middle) 27 February 2010 Chile (M_w 8.8), and (right) 11 March 2011 Tohoku, Japan (M_w 9.0) earthquakes. Regions of largest fault displacements (yellow) and regions of coherent short-period (~1 s) teleseismic radiation (blue) are indicated. The dashed lines are the position of the subduction zone trench, the thick gray lines are coastlines, and the red stars are the epicenters. In each case the coherent short-period radiation comes from downdip, closer to the coast (25–50 km deep), while the large slip zones are in the upper 25 km, extending seaward toward the trench. Short-period energy is located by network back-projections, while main slip regions are located by inverting seismic, geodetic, and/or tsunami observations, as described in the text for each event.

abrupt or gradational, and is influenced by age, temperature, and/or geometry of the subducting plate.

5. Megathrust Faulting Domains

[20] The recently characterized variations in earthquake rupture properties with depth along the seismogenic zone discussed above motivate a conceptual model involving four megathrust domains with different seismic behavior, as depicted in Figure 6. Recognizing that earthquakes are complex phenomena, this conceptual model is intended as a framework for comparing behavior and assessing likely contributing factors manifested in the seismic variability. We introduce this model framework and then evaluate additional observations for both great and moderate size earthquakes in its context.

[21] The shallowest region of the megathrust, labeled domain A, extends from the trench down to about 15 km depth below sea level and experiences either aseismic deformation or large coseismic displacements in tsunami

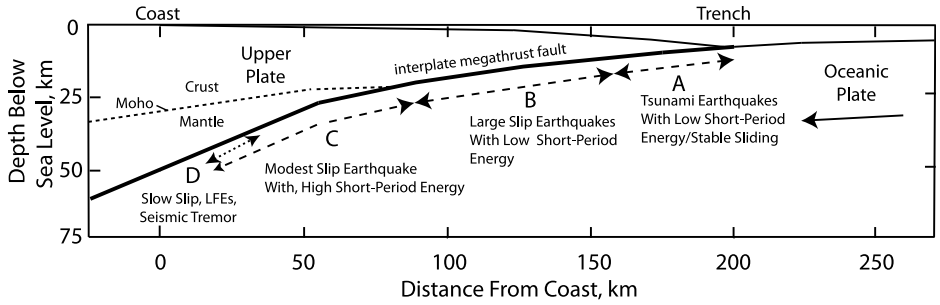

Figure 6. Rupture domains of interplate megathrust faults. Schematic cross-section, scaled appropriately for the subduction zone off the northeast coast of Honshu where the great 2011 Tohoku earthquake occurred, indicating four domains of megathrust rupture characteristics: A – near-trench domain where tsunami earthquakes or anelastic deformation and stable sliding occur; B – central megathrust domain where large slip occurs with minor short-period seismic radiation; C – downdip domain where moderate slip occurs with significant coherent short-period seismic radiation; D – transitional domain, only present in some areas, typically with a young subducting plate and shallow megathrust dip, where slow slip events, low frequency earthquakes (LFEs), and seismic tremor can occur. At yet greater depths the megathrust slides stably or with episodic slow slip or with plastic deformation that does not generate earthquakes.

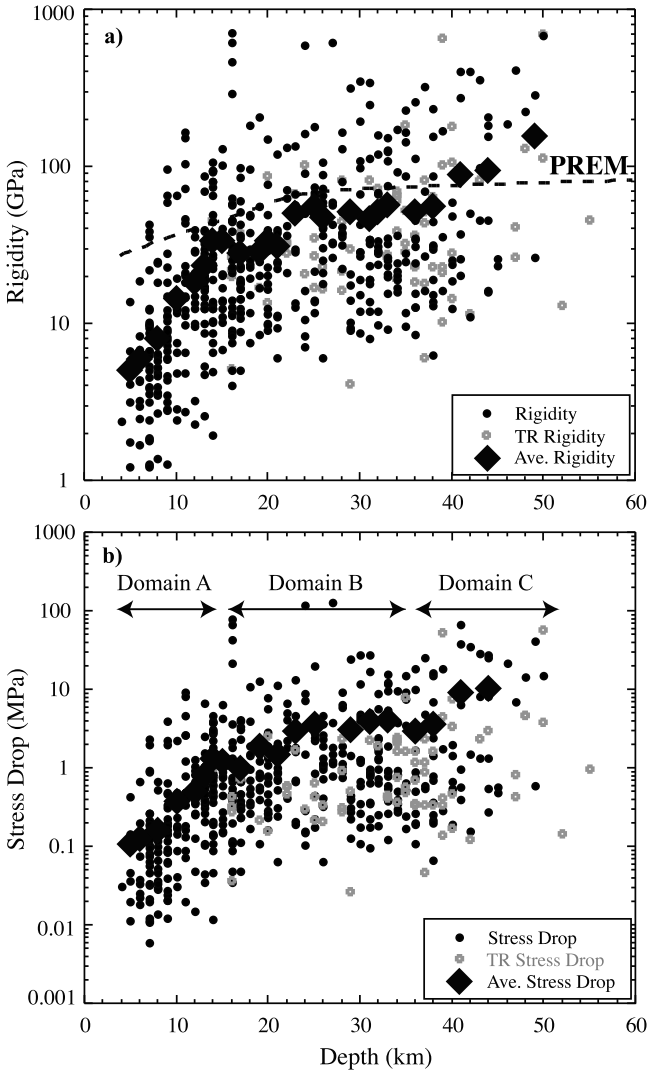

Figure 7. Estimates of source rupture characteristics of interplate thrusting events from globally distributed subduction zones from deconvolved source time functions compiled by *Lay and Bilek* [2007] including studies by *Bilek and Lay* [1999] and *Tanioka and Ruff* [1997] (TR). Source function durations are used to infer (a) source region rigidity (under assumption of constant stress drop), and (b) source static stress drop (under the assumption of constant rupture velocity) and plotted as functions of source depth. Filled diamonds indicate mean values in depth bins. The values of rigidity from PREM [*Dziewonski and Anderson*, 1981] are shown for reference. The approximate depth ranges of the megathrust domains from Figure 6 are indicated.

earthquakes (Figure 6). The 1992 Nicaragua, 2006 Java, and 2010 Mentawai tsunami earthquakes appear to have ruptured across domain A. The 1992 Nicaragua and 2010 Mentawai events appear to have initiated relatively deep in domain A and ruptured updip. While large slip occurs at shallow depth during tsunami megathrust events, it is not clear whether strain is distributed throughout the toe or concentrated at the downdip edge of domain A. The 2011 Tohoku event appears to have nucleated even deeper along the megathrust, with slip extending all the way to the trench in a relatively unusual event.

[22] Great earthquakes in domain B (from 15 to 35 km depth) rupture with large total slip that radiates relatively modest amounts of coherent short-period energy, while large earthquakes that rupture domain C (from 35 to 55 km depth) tend to have moderate slip in this depth range but relatively high amounts of coherent short-period energy. This is a fairly subtle distinction, and evidence for the segmentation in rupture properties derives primarily from the detailed analyses of the 2004 Sumatra (M_w 9.2), 2010 Chile (M_w 8.8) and 2011 Tohoku (M_w 9.0) events described above. Similarly, the distinction between domain A and domain B for the 2011 Tohoku event is rather subjective, but is supported by occurrence of the updip 1896 Sanriku tsunami earthquake to the north [e.g., *Kanamori*, 1972; *Tanioka and Sataka*, 1996], and variation of source time functions for smaller events, as discussed below.

[23] The final megathrust domain (D) is the downdip transitional region where slow slip events, low frequency events, and seismic tremor phenomena have been well-documented for subduction of relatively young plates (Cascadia, Southwest Japan). Domain D may be very narrow, or non-existent in regions with steeper megathrust dip and deeply extending domain C. The proposed megathrust domain framework will now be compared with further observations from both great and large earthquakes to explore its value in characterizing seismic rupture attributes of the seismogenic zone. Much has been written recently about zone D, which has been a focus of study in regions with dense geodetic and local seismic observations [e.g., *Beroza and Ide*, 2011], so here we focus on regions illuminated by global seismic observations, domains A, B, and C.

6. Earthquake Source Variations Across Megathrust Domains

[24] The megathrust domain structure introduced in Figure 6 is based on first-order seismological observations, and it is of interest to evaluate whether the domain subdivision can be validated in terms of quantitative source differences. This is a major challenge, and we provide several types of quantification here. We consider depth-variations in source property estimates, seismic magnitude measures, estimates of ground velocity spectral variations over the fault plane for great ruptures, variations in teleseismic and near-field spectra for moderate size ruptures, and variations in moment-scaled energy release.

6.1. Source Property Variations

[25] The systematic estimation of point-source teleseismic source time functions for many interplate thrust events provides one probe of depth-varying properties of the megathrust regime, as reviewed by *Lay and Bilek* [2007]. Figure 7 shows plots of two source attributes inferred from deconvolved source time function durations scaled to a common seismic moment, for many moderate-size subduction zone thrust events. Because the source finiteness cannot be reliably resolved using teleseismic data for these events, variations in observed source duration do not give unique source properties. The durations can be mapped into seismic rupture

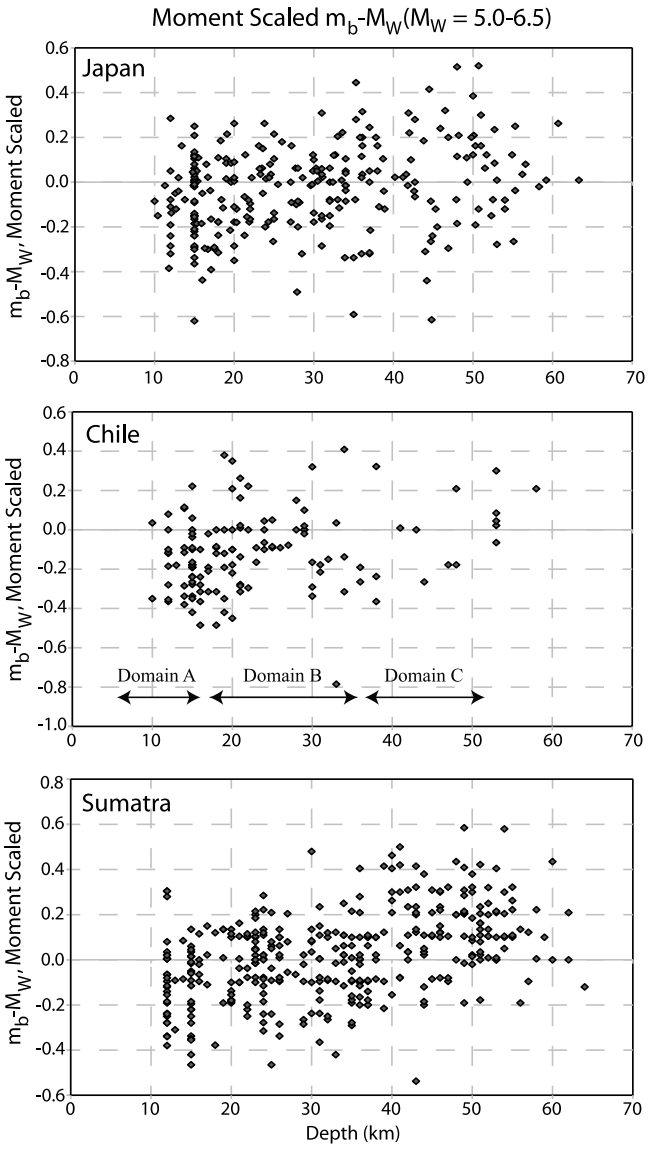

Figure 8. Depth variation of differences in seismic magnitudes m_b-M_w for interplate thrust events on the megathrusts near the (top) 2011 Tohoku, (middle) 2010 Chile, and (bottom) 2004 Sumatra great earthquakes. The magnitude differences have been corrected for corner frequency scaling with seismic moment using an ω-squared source. The m_b values are from the USGS PDE bulletin and the M_w values are from the Global Centroid Moment Tensor catalog. The approximate depth ranges of the domains from Figure 6 are shown on the middle panel. Only events in the range $5 \leq M_w \leq 6.5$ are included to avoid saturation in the m_b measurements due to fixed time window [modified from *Rushing and Lay*, 2011].

velocity variations assuming unilateral slip models and those rupture velocities in turn related to fault zone shear velocity, and hence rigidity variations (Figure 7a). Alternatively, assuming uniformly scaled fault dimensions, the observed source durations can be mapped into static stress drop variations (Figure 7b). In either case–and the reality is likely a mix of both–there is a strong variation of source rigidity and/or stress drop within the depth extent of domain A, gradual change with depth across domain B, and some indication of increase into domain C. While there is substantial variability in data for different regions, most well-sampled subduction zones display similar basic trends [*Bilek and Lay*, 1998, 1999, 2002; *Bilek*, 2007; *Lay and Bilek*, 2007; *Bilek and Engdahl*, 2007]. Extending the data sampling of the deeper portion of the megathrust to better establish whether there is a clear distinction of domain C appears to be a promising undertaking.

6.2. Seismic Magnitude Variations

[26] Analysis of teleseismic source time functions is viable for events with $m_b > 6.0$, but difficult for smaller magnitude events. One approach to extend the size range of events used to evaluate the megathrust domain notion is to use seismic magnitudes, in particular m_b-M_w magnitude differentials. Large scatter is to be expected with any magnitude data set due to regional variations in attenuation, changes in focal mechanism geometry relative to observing network, and many other factors. We limit comparisons of seismic magnitude differentials to the megathrust regions ruptured by the 2004 Sumatra-Andaman, 2010 Chile, and 2011 Tohoku great earthquakes, using USGS NEIC measures of P wave m_b (measured for about 1 s period energy over the first few seconds of the seismic signal) and M_w values from the Global Centroid Moment Tensor (GCMT) catalog. The source locations, depths, and moment tensors were used to identify events likely to be interplate thrust events. In order to avoid biases in the m_b values for large events with longer than several second rupture durations, we limit the analysis to events with m_b 5.0 to 6.5. Even across that magnitude range there is some expected scaling of the 1 Hz energy level relative to seismic moment, and we apply a correction to the magnitude differentials for moment scaling of an ω-squared source spectrum with a 3 MPa constant stress drop [*Rushing and Lay*, 2011].

[27] Figure 8 shows the resulting moment-scaling corrected m_b-M_w measurements as a function of GCMT centroid depth for the three megathrust regions [*Rushing and Lay*, 2011]. There is a weak increase in m_b-M_w with depth for the Japan zone, possibly a comparable increase, albeit sparsely defined, for central Chile, and a relatively clear trend (or step increase around 37 km depth) for northern Sumatra. Similar plots are found using hypocentral depth estimates from the NEIC or the Joint Metrological Agency (JMA); the GCMT depths tend to have less scatter relative to the megathrust trend although they are ~10 km deeper overall. The central portion of the fault (domain B) tends to have average differentials around zero, consistent with the empirical agreement of m_b and M_w for events with M_w ~5 (source durations ≤1 s) [*Utsu*, 2002]. Some distinction of domain A may be apparent for Sumatra, but the large scatter obscures any clear distinction for the other two regions. There are relatively few moderate size events with very shallow depths near the toe of the megathrusts, which is probably a manifestation of the conditionally stable, or completely locked conditions there. *Rushing and Lay* [2011] consider similar magnitude differential patterns for other regions near large earthquakes without finding great consistency in trends, but few other regions have the exceptionally wide seismogenic zones of the events in Figure 8.

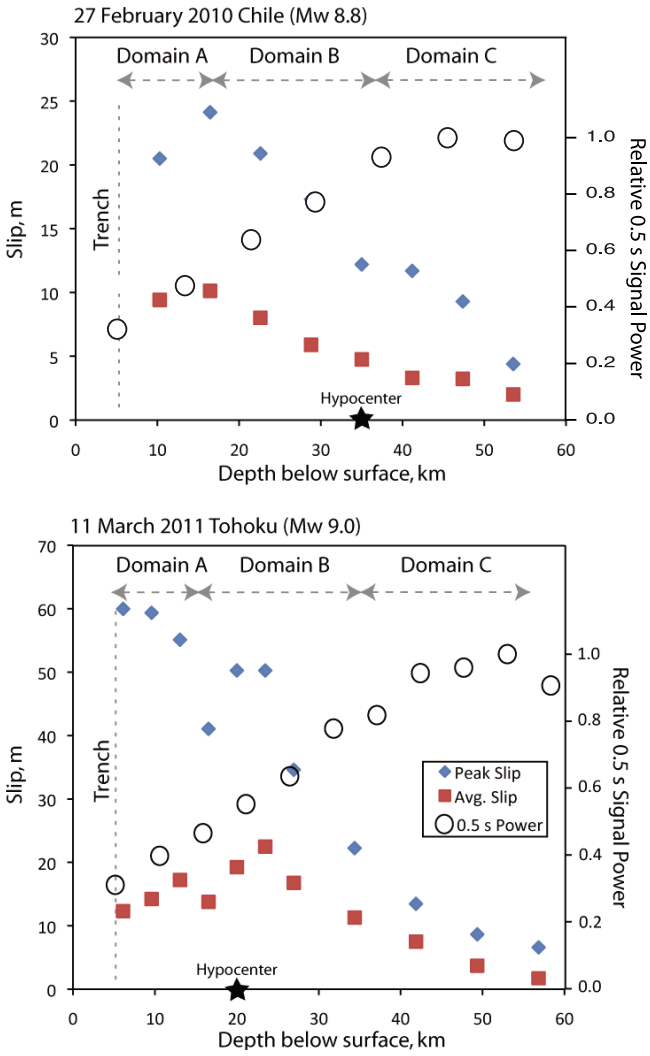

Figure 9. Peak and average slip along strike from the finite-source rupture models shown in Figure 1, and relative 0.5 s teleseismic short-period P wave energy averaged along strike from USArray observations for the great (top) 2010 Chile and (bottom) 2011 Tohoku megathrust ruptures. The stars indicate the hypocentral depth for each event, and the approximate extent of the rupture domains from Figure 6 are indicated, along with the position of the trench.

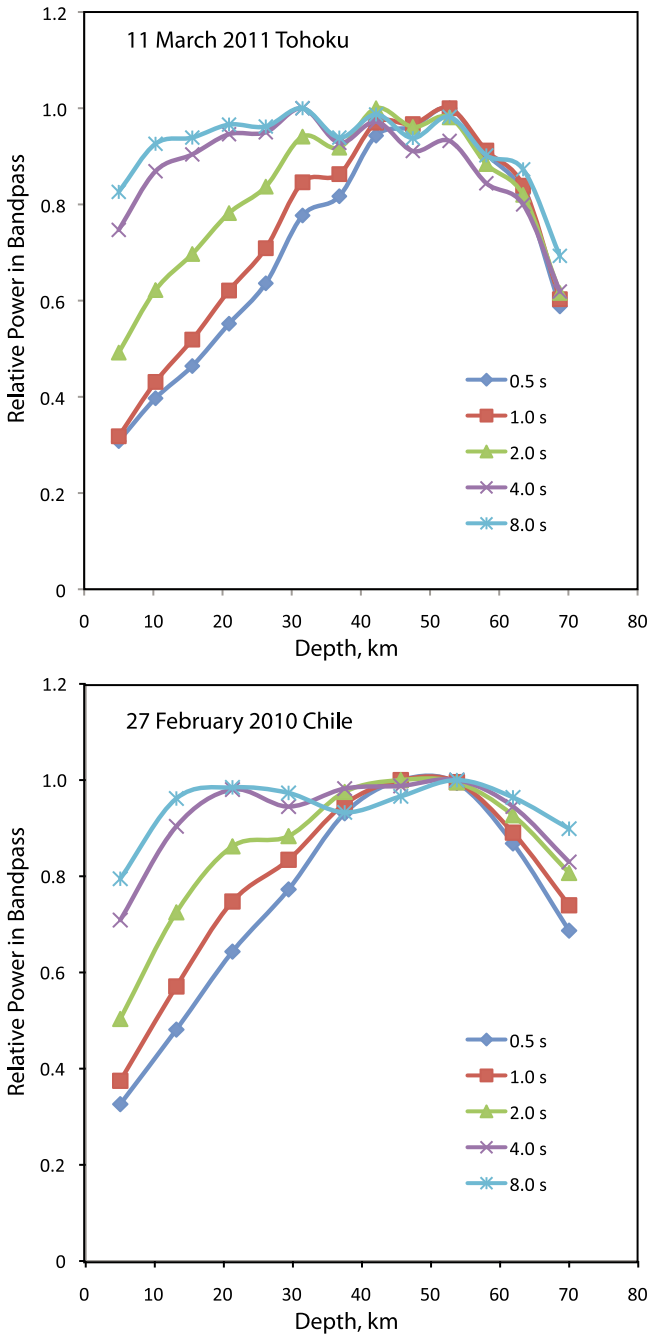

Figure 10. Relative ground velocity power for different narrowband filters of teleseismic P waves recorded by the Transportable Array back-projected to the source regions of the (top) 2011 Tohoku and (bottom) 2010 Chile great earthquakes. The peak amplitude of the along-strike averaged signal power for each depth bin is normalized in each passband. This emphasizes the relative depletion of shorter period energy radiated from shallower depths of the megathrust during these two immense events. The drop off of energy below 55 km depth indicates the degree of depth smearing of the power estimates for all bandwidths due to the back-projection processing.

6.3. Teleseismic Ground Velocity Variations for Great Events

[28] The comparisons of teleseismic short-period back-projection and finite-fault slip inversions for recent great events in Figures 1 and 5 indicate differences in spectral content, but the nature of the processing obscures the absolute levels of the spectral differences. Quantifying the radiation spectrum across the megathrust for great events is very difficult; finite-fault inversions determine slip distribution for relatively long periods (>5 s), and back-projection waveform stacking isolates regions of coherent short-period (<5 s) radiation, but that does not provide a complete spatial mapping of the spectral variations. Most back-projection analyses focus on the peak interference patterns, as they

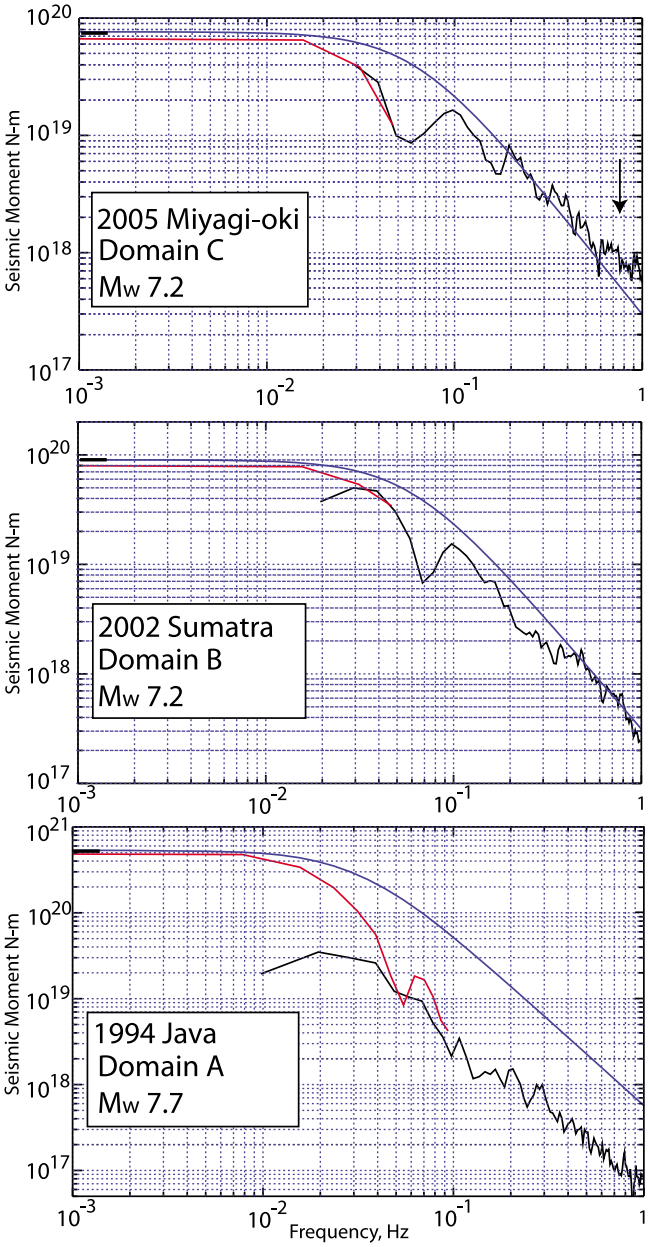

Figure 11. The averaged source spectra of far-field P waves for moderate size earthquakes rupturing entirely within each of the three megathrust domains identified in Figure 6. The blue lines indicate a reference Brune-source ω-squared spectrum computed for the event seismic moment, Mo, a shear velocity of 3.75 km/s, and a stress drop of 3 MPa. The corresponding corner frequencies are 0.062 Hz, 0.059 Hz and 0.033 Hz for the (top) 2005, (middle) 2002, and (bottom) 1994 events, respectively. The red lines are the observed spectra obtained from finite-fault models for each event and the black lines are the observed spectra estimated from broadband teleseismic P waves. The arrow highlights the enriched short-period signal amplitude for the domain C event.

represent the most coherent imaging by short-period signals, but the back-projections include spatial projections of short-period signal over the entire fault surface, filtered with a coherency filter of some form.

[29] We consider linear stacking (rather than fourth-root stacking) to estimate relative power distribution for 0.5 s ground velocity of teleseismic P waves recorded by the USArray, back-projected to the 2010 Chile and 2011 Tohoku source regions and averaged along-strike in depth bins is shown in Figure 9. The absolute amplitude of the stack is normalized to unity, as we do not have reliable control on azimuthally averaged source amplitude spectra. These values are shown relative to the along-strike peak and average slip from teleseismic body wave finite-fault rupture models [*Lay et al.*, 2010b, 2011a]. As noted earlier, geodetic inversions tend to place slip somewhat closer to shore than some seismic inversions for both events, but the seaward extent of rupture is not well-resolved. Peak slip values are located in domain A for both events, but the average slip peaks in domain B for the Tohoku event. The low level of 0.5 s period seismic energy originating in domain A is clear, as is the peak of this signal in domain C. The smoothness of the trends with depth partly reflects intrinsic limitations of the imaging methods, and one would not expect sharp domain boundaries to be evident in these figures even if they are actually present.

[30] Figure 10 is a plot of the frequency dependent variations of the back-projected short-period signal from USArray for the same events, using a similar procure. The peak of each passband is normalized to unity to clarify the relative depletion of short-period signal from the shallower portion of the rupture plane. The absolute levels of power for the different passbands differ by many orders of magnitude, with very low power at shorter periods. This indicates that spectral slope differences as a function of depth, while systematic, are minor. At a period of 8 s the distribution is relatively flat with depth (this still indicates a shallow deficit relative to the slip distributions as seen in Figure 9) and there is no depth resolution at all for longer periods. The degree of spatial smearing of the reconstructed energy source is indicated by the fall-off of energy imaged below 55 km, where there was little or no co-seismic slip.

6.4. Source Spectrum Variations

[31] Back-projection procedures give an intrinsically biased view of the source spectrum, as they are designed to detect and enhance coherent subsources, and often use nonlinear stacking that distorts amplitudes. Usually, corrections for radiation pattern, attenuation, and site response are not included in back-projections, so absolute amplitudes are not recovered. Consideration of azimuthally averaged ground displacement spectra should further clarify the subtle energy contributions of the shorter period signals. Figure 11 shows averaged P wave displacement spectra for moderate size events that ruptured entirely within single megathrust domains. Reference spectra for conventional seismic moment and corner frequency scaling are shown in each case. The spectra for events rupturing in different domains have only subtly different high frequency slopes in the passband 0.1–1.0 Hz, with the 16 August 2005 Miyagi-oki (M_w 7.2) earthquake representing domain C having relative enrichment of spectral amplitudes above 0.3 Hz. The short-period enrichment for slip in domain C is thus systematic for both events with ruptures confined to that domain and for great ruptures that also span shallower domains like the 2010 Chile and 2011 Tohoku events. It is not clearly established

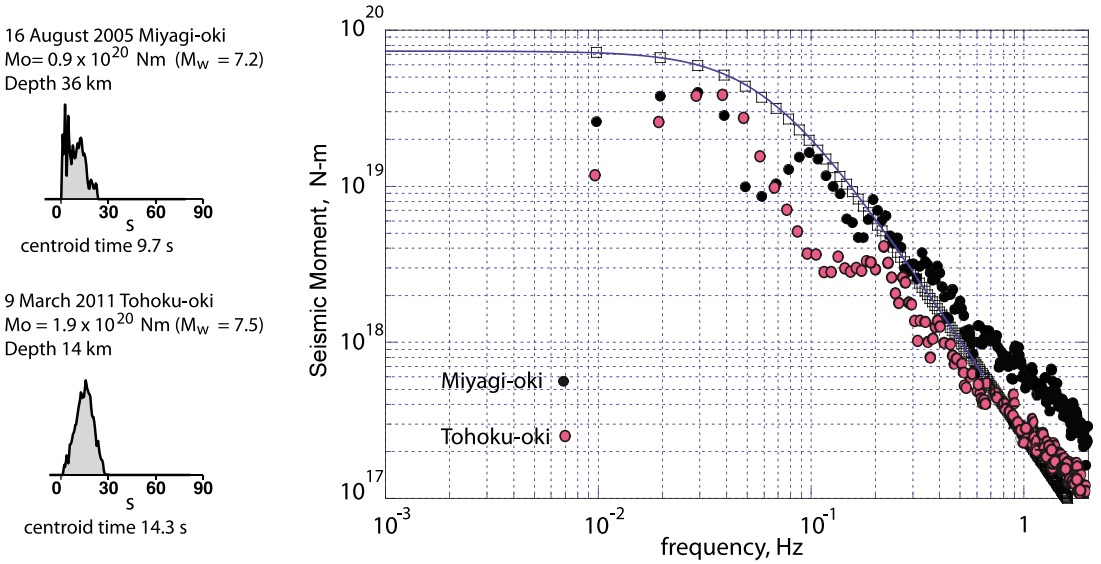

Figure 12. Comparison of the source time functions and averaged source spectra of far-field P waves for two large earthquakes offshore of Honshu, Japan. The 16 August 2005 Miyagi-oki (GCMT M_w = 7.2) earthquake has a rougher source time function obtained by finite-fault inversion of teleseismic P waves than the 9 March 2011 Tohoku-oki (GCMT M_w = 7.3) earthquake, which was a foreshock two days before the 11 March 2011 Tohoku earthquake. The 2005 event has a centroid depth near 36 km, and would be designated a domain C event, whereas the 2011 event is significantly shallower. The inversion here assumed a GCMT depth of 14 km, but analysis of ocean bottom seismometer data indicates that the event actually has a hypocentral depth of 23 km [*Suzuki et al.*, 2012] and would be designated a domain B event. The source spectra indicate that the Miyagi-oki event has higher spectral amplitudes (black dots) over the passband 0.1 to 2.0 Hz, than the somewhat larger Tohoku-oki event (red dots). The boxes indicate the nominal ω-squared spectrum for the seismic moment of the 2005 event, similar to those shown in Figure 11.

whether this is a manifestation of differences in rupture mode or superposition of additional radiation from small-scale subevents during rupture of domain C. Domain A events, here represented by the 2 June 1994 Java (M_w 7.7) tsunami earthquake, are significantly shifted in corner frequency relative to conventional spectra and the other domains, but do not have anomalous high frequency spectral slopes. The shift of corner frequency is consistent with the measured low rupture velocities for recent tsunami earthquakes, although *Abercrombie et al.* [2001] use a moderate rupture speed of 2 km/s for the 2 June 1994 event. These comparisons indicate that if true spectral amplitudes could be reliably estimated as a function of depth along the megathrust for the data in Figures 8 and 9, very strong overall variations would be found for large events. *Allmann and Shearer* [2009] find only a weak increase in stress drop from 30 to 50 km depth, in a global compilation of spectral shapes, noting that the increase is primarily associated with subduction zone events.

[32] Source attributes for two events located offshore of Honshu, Japan are compared in Figure 12. The 2005 Miyagi-oki (M_w 7.2) spectrum from Figure 11 is extended to 2 Hz, and compared with the 9 March 2011 (M_w 7.3, GCMT) foreshock to the great 2011 Tohoku rupture. The latter event is updip on the megathrust from the 2005 event, and falls into domain B. Teleseismic P waves were inverted for finite-source models for the two events, and the resulting source time functions are shown. The 2005 event has a smaller centroid time and a significantly rougher moment rate function, although both models were parameterized equivalently. The averaged source spectra for the two events shows that the 2005 earthquake has higher spectral amplitudes at short-periods, consistent with the behavior between domains seen in Figure 11, with some indication that this difference increases with increasing frequency.

[33] To provide a connection between the teleseismic observations and regional strong-ground motions, we analyzed the three-component recordings from 62 K-net and 50 Kik-net stations in Iwate (153 channels), Miyagi (72 channels) and Fukushima (110 channels) Prefectures for the two events considered in Figure 12. Figure 13 indicates the locations of the sources and three clusters of stations in each Prefecture. Record lengths of up to 150 s of the ground accelerations were demeaned, tapered, and spectral ratios were computed component by component with the spectra from the 2005 event being divided by the spectra from the 2011 event. The individual spectral ratios were smoothed with a 9 sample running mean and the ratios were averaged over all components to give the average spectral ratios shown here. No explicit corrections for differences in path length were applied, as these are whole-signal spectra and the frequency-dependent attenuation structure is not known in detail. The 20 km greater source depth for the 2005 event reduces path length differences, and for the Iwate stations the path length differences are rather small. All three azimuthally distributed network average spectral ratios show a similar increase in ground acceleration spectra with increasing frequency for the 2005 domain C event relative to the

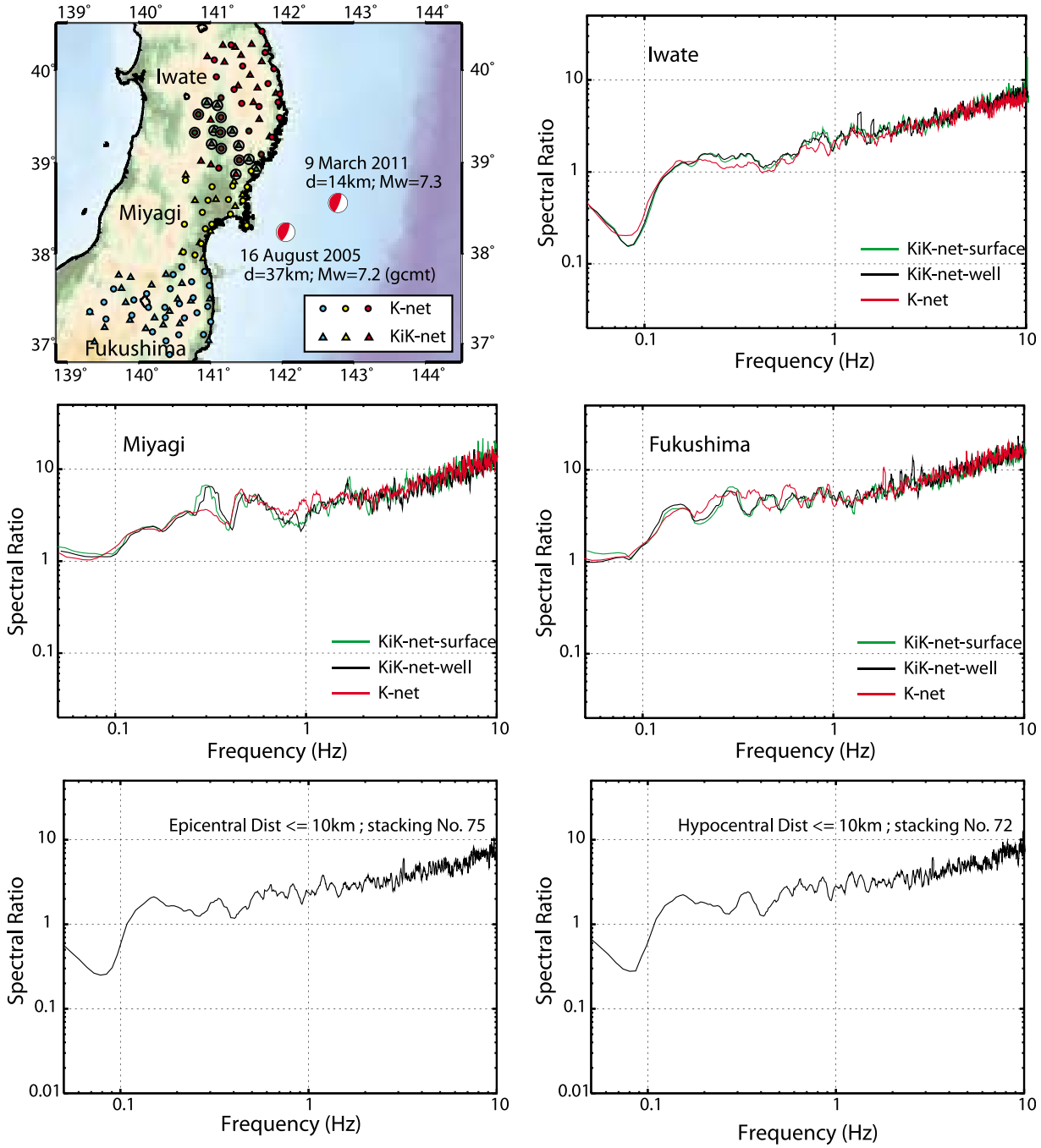

Figure 13. Spectral ratios between the 16 August 2005 Miyagi-oki (M_w 7.2) and 9 March 2011 (M_w 7.3) earthquakes from K-net and Kik-net strong motion sensors in Iwate, Miyagi, and Fukushima prefectures (map). The stacked, smoothed spectral ratios (2005 event/2011 event) from all three components of recorded ground accelerations over 150 s windows are shown, with separate averages computed for K-net and KiK-net observations. The deeper 2005 Miyagi-oki event has systematically higher amplitude acceleration spectra relative to the 2011 Tohoku-oki event as frequency increases above 0.1 Hz, consistent with the far-field source spectra for the two events shown in Figure 12.

2011 domain B event. This pattern is similar to that apparent in the teleseismic source spectra up to 2 Hz, but here extends to 10 Hz. This correspondence reinforces the likelihood that the trends in Figure 13 are not completely controlled by path effects. Assuming that the great 2011 Tohoku (M_w 9.0) event ruptured domains A, B and C with corresponding differences in high frequency radiation to that apparent in Figure 13, it is consistent that *Kurahashi and Irikura* [2011] locate sub-sources of strong-ground motion energy radiation in the downdip, domain C region (Figure 1). Ongoing work to develop path corrections and map out variations in strong motion source radiation for additional events using the

Table 1. Large Earthquake E_r/M_o

Event	M_w	M_o (Nm)	E_r	E_r/M_o (10^{-6})
11 March 2011 Tohoku	8.99	3.90×10^{22}	4.18×10^{17}	10.72
25 October 2010 Mentawai	7.82	6.66×10^{20}	1.41×10^{15}	2.12
6 April 2010 Sumatra	7.76	5.56×10^{20}	4.80×10^{15}	8.6
27 February 2010 Chile	8.78	1.84×10^{22}	2.10×10^{17}	11.41
20 February 2008 Sumatra	7.30	1.12×10^{20}	1.01×10^{15}	9.00
12 September 2007b Sumatra	7.86	7.76×10^{20}	8.90×10^{15}	11.47
12 September 2007b(1) Sumatra	7.63	3.52×10^{20}	6.50×10^{15}	18.47
12 September 2007a Sumatra	8.40	5.05×10^{21}	4.40×10^{16}	8.71
15 August 2007 Peru	7.96	1.11×10^{21}	1.70×10^{16}	15.32
1 April 2007 Solomon Islands	8.07	1.60×10^{21}	1.05×10^{16}	6.56
15 November 2006 Kuril Islands	8.29	3.40×10^{21}	1.62×10^{16}	4.76
17 July 2006 Java	7.71	4.61×10^{20}	3.80×10^{14}	0.82
16 August 2005 Miyagi-oki	7.18	7.40×10^{19}	5.48×10^{14}	7.41
28 March 2005 Sumatra	8.63	1.10×10^{22}	8.20×10^{16}	7.45
26 December 2004 Sumatra	9.14	6.50×10^{22}	2.98×10^{17}	4.59
25 September 2003 Tokachi-oki	8.26	3.05×10^{21}	1.89×10^{16}	6.20
2 November 2002 Sumatra	7.24	9.01×10^{19}	8.87×10^{14}	9.80
23 June 2001 Peru	8.38	4.67×10^{21}	3.99×10^{16}	8.54
2 June 1994 Java	7.75	5.30×10^{20}	1.35×10^{15}	2.55
2 September 1992 Nicaragua	7.62	3.40×10^{20}	3.71×10^{14}	1.09

extensive K-net and Kik-net regional strong motion networks and Hi-net stations is being pursued, but for our purpose here, the correspondence between teleseismic and regional source radiation differences between megathrust rupture domains is established.

6.5. Moment-Scaled Energy Variations

[34] Determination of total radiated seismic energy, E_r, scaled by seismic moment, M_o, as a function of depth along the megathrust is a desirable approach to quantifying rupture behavior [e.g., *Newman and Okal*, 1998; *Venkataraman and Kanamori*, 2004; *Rivera and Kanamori*, 2005; *Convers and Newman*, 2011]. This provides a quantitative characterization of the rupture processes, but can isolate behavior for each domain only to the extent that a rupture is confined to a specific depth range. A global analysis of 342 events with $M_w \geq 6.7$ suggests both regional and overall increases in $\log_{10}(E_r/M_o)$ with source depth for thrust events, albeit with the large scatter characteristic of radiated energy measurements [*Convers and Newman*, 2011].

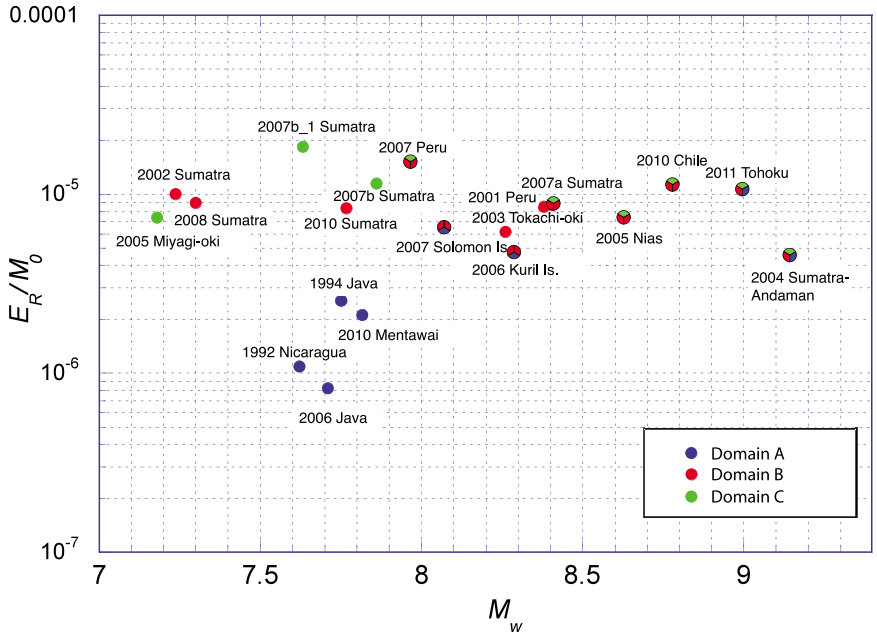

Figure 14. Estimates of radiated seismic energy scaled by seismic moment, from teleseismic P wave ground velocity spectra and broadband source time functions from finite source inversions for recent large earthquakes. All events shown are megathrust ruptures, color-coded to indicate the rupture domains spanned by the rupture. The blue dots indicate tsunami earthquakes that rupture the shallow domain A, with characteristic low E_R/M_o ratios. The red dots indicate ruptures of domain B, and the green dots indicate ruptures of domain C. Multicolor dots indicate rupture of more than one domain with dominant color indicating the primary domain.

Table 2. Large Earthquake Rupture Domains and E_r/M_o

Event	M_w	Domains	E_r/M_o (10^{-6})
11 March 2011 Tohoku	9.0	ABC	10.72
25 October 2010 Mentawai	7.8	A	2.12
6 April 2010 Sumatra	7.8	B	8.6
27 February 2010 Chile	8.8	BC	11.41
20 February 2008 Sumatra	7.3	B	9.00
12 September 2007b Sumatra	7.9	C	11.47
12 September 2007b(1) Sumatra	7.6	C	18.47
12 September 2007a Sumatra	8.4	B(C)	8.71
15 August 2007 Peru	8.0	BC	15.32
1 April 2007 Solomon Islands	8.1	(A)B	6.56
15 November 2006 Kuril Islands	8.3	(A)B	4.76
17 July 2006 Java	7.8	A	0.82
16 August 2005 Miyagi-oki	7.2	C	7.41
28 March 2005 Sumatra	8.6	BC	7.45
26 December 2004 Sumatra	9.2	ABC	4.59
25 September 2003 Tokachi-oki	8.3	B	6.20
2 November 2002 Sumatra	7.2	B	9.80
23 June 2001 Peru	8.4	B	8.54
2 June 1994 Java	7.7	A	2.55
2 September 1992 Nicaragua	7.6	A	1.09

[35] Table 1 lists our radiated energy measurements made for many large, well-recorded megathrust events. Estimates of the radiated energy for frequencies less than ~0.1 Hz were made using moment rate functions from finite-fault models inverted from teleseismic body wave observations. Broadband teleseismic P wave ground motion velocity spectra were used for estimating radiated energy for frequencies in the range of 0.1 to 1.0 Hz. The seismic moment, M_o, was used to constrain the moment rate functions at very low frequency. The total radiated energy, E_r, was then divided by the seismic moment. The basic analysis procedures follow published theory and methods of *Venkataraman and Kanamori* [2004] and *Rivera and Kanamori* [2005]. The energy estimates are most affected by uncertainties in source depth, which affects the P wave and S-wave velocities used in the energy estimates. There are also uncertainties associated with data bandwidth and propagation corrections.

[36] Moment-scaled radiated energy measures are shown in Figure 14 for recent large interplate earthquakes, with symbols identifying the megathrust domain(s) that ruptured. The appendix discusses each of the events and the basis for assigning rupture domain(s) to each event, as listed in Table 2. The large tsunami earthquakes that rupture domain A have distinctly low moment-scaled radiated energy levels. Great events that rupture across domains A, B, and C have average energy levels, and it is difficult to partition energy to each domain. Domains B and C can fail largely independently in large events (Table 1); the 28 March 2005 Sumatra earthquake (M_w 8.6) ruptured B, and possibly C (Figure A1); the 12 September 2007 Kepulauan (M_w 7.9) earthquake ruptured C while the adjacent 12 September 2007 Sumatra (M_w 8.5) earthquake primarily ruptured B but with some deep short-period radiation from domain C (Figure A1); the relatively small (M_w 7.4) 1978 and 2005 Miyagi-oki earthquakes ruptured the same region of C that re-ruptured in the 2011 Tohoku with strong short-period radiation. Domains A and B can fail together as well, as appears to be the case for the 15 November 2006 Kuril Islands (M_w 8.4) and 1 April 2007 Solomon Islands (M_w 8.1) events, both of which ruptured to very shallow depth. There is rather subtle difference in energy characteristics for domains B and C, with the latter having only modestly increased energy levels in general. Figure 11 indicates that the differences in spectral amplitudes are systematic, but only pronounced for the shortest periods, for which the fraction of total energy contributed up to 1 Hz is modest, so the lack of a stronger distinction in Figure 14 is understandable. The previous section on spectral analysis suggests that the high frequency slope of the spectrum is less steep for domain C events, thus, energy from high frequencies may be most underestimated for the deeper events. Unfortunately, uncertainty of teleseismic P wave attenuation for frequencies above 1 Hz precludes confident analysis of the corresponding energy.

[37] The rupture domain assignments are intrinsically somewhat subjective; great earthquakes are complex and not easily categorized by simple metrics. However, the recent large events have been well-recorded and first-order features revealed by extensive studies of their source processes (Appendix A) guide our designations.

7. Discussion

[38] Displacement across a fault can occur with a broad spectrum of slip rates, ranging from stable sliding or episodic creep to abrupt stick-slip earthquake faulting. Efforts to account for the variable failure processes have largely involved consideration of fault frictional strength and ability to accumulate large strains/stresses prior to failure, combined with consideration of stability, where variables such as pressure, temperature and pore fluid presence control slip-velocity strengthening or weakening behavior, resulting in stable sliding or unstable earthquake behavior, respectively [e.g., *Heaton*, 1990; *Scholz*, 1998; *Zheng and Rice*, 1998; *Ben-Zion*, 2001]. Transitional zones of conditional stability may separate these regions, in which stable sliding occurs at low strain rates, but unstable sliding can occur during transient high strain rates. Earthquake ruptures can then propagate into otherwise stable regions even if they are unable to nucleate in them. Our characterization of megathrust failure domains and their seismic radiation distinctions provides new context for these considerations.

[39] The corner frequency of source spectra is a manifestation of finite time scales in the rupture, including total rupture duration (influenced by rupture velocity), and particle dislocation risetime (time scale of sliding at a point on the fault). Observationally, it is very difficult to resolve precise sliding time-histories at localized positions on a fault; the risetime is obscured by both wave propagation effects and rupture area expansion. The data for the 2011 Tohoku earthquake are the best available for any great megathrust rupture, and we find that the risetime for the regions with 40–60 m of slip are on the order of 20–30 s [*Yue and Lay*, 2011], giving average estimated fault sliding velocities of ~2 m/s for this event's rupture of domains A and B. Higher particle velocities may have occurred locally. We also estimate a lower bound of about 1.5 km/s for the rupture velocity in these regions. Quantification of corresponding parameters for other events is limited due to severe trade-offs in the modeling of exclusively far-field observations. Offshore geodetic measurements during rupture growth will be needed to overcome the trade-offs between rupture expansion rates and slip risetime for future

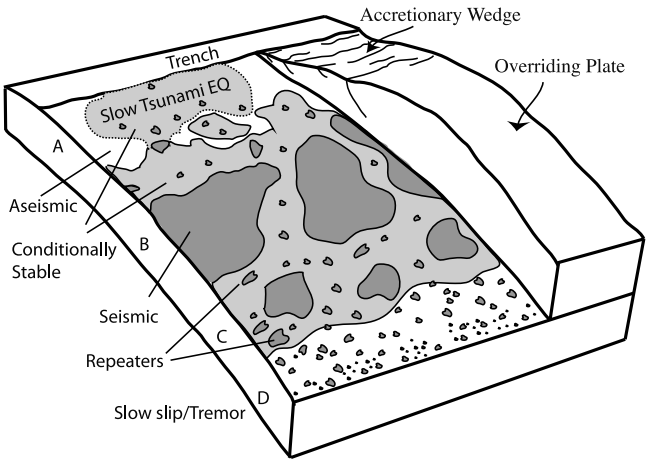

Figure 15. Cut-away schematic characterization of the megathrust frictional environment, related to domains A, B, C and D defined in Figure 6. Regions of unstable frictional sliding are dark regions labeled "seismic." Regions of aseismic stable or episodic sliding are white regions labeled "aseismic." Medium gray areas are conditional stability regions, which displace aseismically except when accelerated by failure of adjacent seismic patches. Domain A is at shallow depth where sediments and pore fluids cause very slow rupture expansion even if large displacements occur in tsunami earthquakes. Domain B has large, relatively uniform regions of stable sliding that can have large slip, but generate modest amounts of short-period radiation upon failure. Domain C has patchy, smaller scale regions of stable sliding surrounded by conditionally stable areas. When these areas fail, coherent short-period radiation is produced. Small, isolated patches may behave as repeaters when quasi-static sliding of surrounding regions regularly load them to failure. Domain D is dominated by aseismic sliding, but many small unstable patches can rupture in seismic tremor when slow slip events occur or when dynamically loaded by tides or shaking from passing seismic waves.

megathrust events. This will be important to quantifying the causes of the rupture differences in the megathrust domains that we have identified.

[40] The 2011 Tohoku event has a larger than typical stress drop (>10 MPa), indicating unusually high stress levels in domain B for that rupture, possibly associated with structural heterogeneity [*Zhao et al.*, 2011]. Variations in roughness on fault and background stress on the rupture surface influence the seismic radiation directly. Contrasts in properties across the fault can affect the rupture dynamics as well, and the increase in seismic velocities with depth is likely to cause increasing rupture velocity with depth, which can affect the corner frequency. As indicated in Figure 6, the most likely fault zone material contrast is the transition along the Japan coast from crust-crust contact to crust-mantle contact, but this transition occurs deeper for the Chile rupture zone, so it is not the sole feature defining domain C. High driving stresses and 'patchy' frictional heterogeneity may account for the enhanced coherent short-period radiation from failures in domain C. While the only comparison with location of sources of strong ground motions is for the 2011 Tohoku event, in that case the teleseismic short-period radiation appears to emanate from the same location as for the local strong ground accelerations. This is supported by the strong motion spectra from moderate size events having enriched short-period amplitudes for domain C events relative to domain B events (Figure 13).

[41] These general ideas are consolidated into a schematic of fault sliding heterogeneity in Figure 15. Systematic depth variations in the extent of seismic versus conditionally stable/aseismic sliding define the properties of the various megathrust domains. This model is essentially an update of the 2D fault description provided by *Scholz* [1998], augmented to recognize the expanding extent of tsunami earthquake occurrence, the distinct short-period radiation characteristics of the deeper portion of the seismogenic interface, and the transitional environment observed at least in regions with young subducting lithosphere. Qualitatively similar conceptual models have been advanced for the Japan subduction zone by *Yamanaka and Kikuchi* [2004], *Uchida and Matsuzawa* [2011] and *Ye et al.* [2012] to explain the distribution of large earthquakes and observations of small repeating earthquakes [e.g., *Shimamura et al.*, 2011] loaded by surrounding zones of quasi-static slip. The precise nature of the seismic asperities and conditional stability properties are not resolved at this time, but this appears to be a useful framework for characterizing depth-dependent properties of megathrust faults.

8. Conclusions

[42] Seismic wave observations of large and great earthquakes on subduction zone megathrusts provide accumulating evidence for systematic depth-dependence of rupture properties. We draw upon analyses of tsunami earthquakes, frequency-dependent rupture characteristics of recent great earthquakes, and observations of slow slip and tremor phenomena to define 4 domains of seismogenic behavior along megathrusts. The shallowest domain A, extends from the trench to about 15 km below sea level, and is a region where aseismic displacement can occur, but large tsunami earthquakes can rupture as well. Large and moderate size events in domain A tend to have longer rupture durations than do deeper events with the same seismic moment, and rupture velocities have been found to be slow for tsunami earthquakes. These events have depleted short-period energy and low moment-scaled seismic energy release. Domain B extends over the depth range 15–35 km, and has great events with large slip but diffuse short-period energy, average seismic magnitude and spectral behavior for smaller events, and average moment-scaled seismic energy release for large events. Domain C extends from 35 to 55 km depth, where increases in megathrust dip are common as are changes from crust-crust to mantle-crust rock contrasts across the fault. Large events in domain C tend to have enhanced short-period energy both teleseismically and in local strong ground motions, and great events that rupture into this region from shallower depth have localized regions of strong coherent short-period seismic radiation. There is some indication of increase in m_b-M_w differential magnitudes in this depth range, as well as relatively high moment-scaled radiated seismic energy release. Young subducting plates with

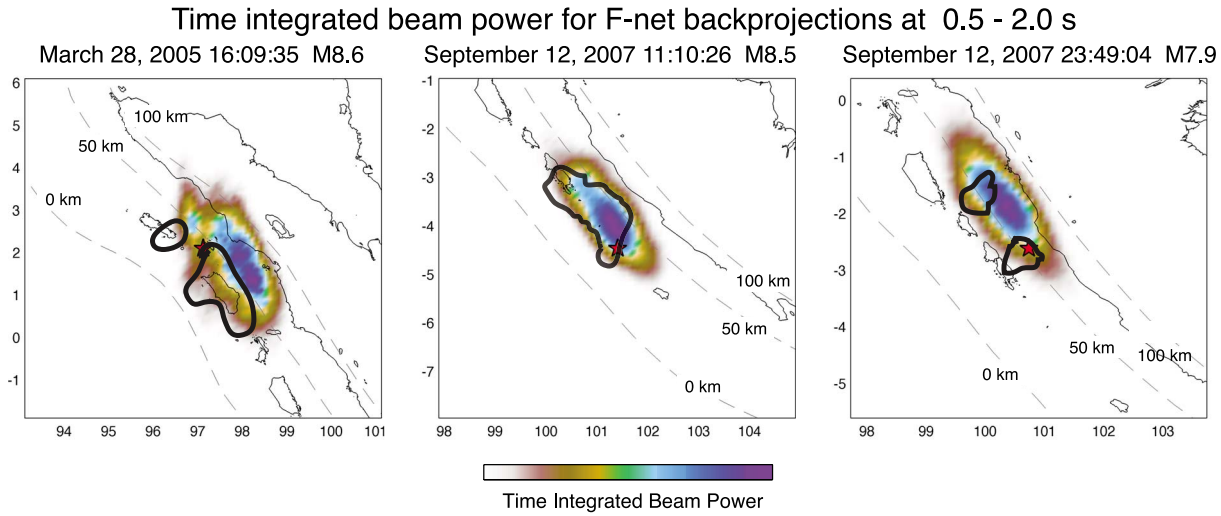

Figure A1. Maps of time-integrated back-projected teleseismic P wave beams at each grid point in the source region of the (left) 28 March 2005 (M_w 8.6), (middle) 12 September 2007 (M_w 8.5), and (right) 12 September 2007 (M_w 7.9) Sumatra earthquakes for data from F-net stations in Japan. The data were filtered in the passband 0.5–2.0 s. The USGS epicenters are indicated by red stars. Dashed contour lines indicate the trench (left-most contours), and slab depths of 50 km and 100 km as defined by the approximate top of the seismogenic zone. Regions of strong slip determined by analysis of seismic and geodetic data are outlined in solid black curves [*Konca et al.*, 2007, 2008]. The 2005 event appears to have ruptured both domains B and C, while the 2007 events ruptured domains B (M_w 8.5 event) and C (M_w 7.9 event).

shallow dip angles appear to preferentially develop a domain D transitional environment at depths of 30–45 km that has a mix of slow slip, low frequency earthquakes, and seismic tremor. Whether this region is present in most subduction zones is not yet established, but no domain D behavior has been reported for the regions of recent great earthquakes where older plates are subducting. Depth variations in the relative proportion of seismic and conditionally stable/aseismic sliding properties of the fault can be invoked to account for the domain segmentation. Fully quantifying the specific mechanisms governing the behavior of each megathrust domain is the challenge for the future.

Appendix A: Rupture Characterizations and Domain Designations for Additional Recent Large Megathrust Earthquakes

[43] Relevant aspects of additional large earthquakes that are incorporated into the megathrust domain categorizations and for which moment-scaled energy has been calculated are summarized here. Designation of which megathrust domain was ruptured by each event is somewhat subjective, and we briefly discuss the rupture attributes of each event that guide our designations.

[44] 12 *June* 1978 *Miyagi* (M_w 7.4, m_b 6.7): This is a moderate size event offshore of the Honshu coastline in the downdip region of the 11 March 2011 Tohoku earthquake that ruptured with strong short-period radiation. It ruptured the same general region as the 16 August 2005 earthquake. The rupture process documented by seismic wave analyses [*Seno et al.*, 1980; *Kanamori et al.*, 2006] indicates that this is a rather typical event rupturing domain C. The data are not reliable enough to determine an E_r/M_o ratio with resolution comparable to that for other events here.

[45] 2 *September* 1992 *Nicaragua* (M_w 7.6, *Ms* 7.2, m_b 5.3): The 1992 tsunami earthquake offshore of Nicaragua ruptured a narrow shallow region close to the trench, in domain A. This event was shown to have relatively low rupture velocity and long source duration, and had very weak short-period radiation and low seismic intensity on the coast [*Kanamori and Kikuchi*, 1993; *Imamura et al.*, 1993; *Velasco et al.*, 1994; *Satake*, 1994]. It has one of the lowest observed E_r/M_o ratios.

[46] 2 *June* 1994 *Java* (M_w 7.8, *Ms* 7.2, m_b 5.7): This event ruptured the shallow domain A region southeast of Java [*Abercrombie et al.*, 2001] and is considered to be a tsunami earthquake, although it has a rather simple source time function comprised of a single dominant pulse. The source depth is somewhat uncertain, with waveform modeling being consistent with 18–22 km deep, but the strong tsunami excitation and the occurrence of many shallow normal faulting aftershocks in the overlying wedge favors rupture in the upper portion of the megathrust.

[47] 23 *June* 2001 *Peru* (M_w 8.4, m_b 6.4): The rupture for this event appears to have initiated with a weak subevent followed by a much larger subevent about 100 km to the southeast [*Lay et al.*, 2010a]. The primary slip zone is in the central portion of the offshore megathrust, within domain B.

[48] 2 *November* 2002 *Sumatra* (M_w 7.4, m_b 6.2): This event ruptured just north of Simeuleu Island, Indonesia, near the 20 February 2008 event. It appears to have ruptured within domain B.

[49] 25 *September* 2003 *Tokachi-oki* (M_w 8.3, m_b 7.0): This great earthquake ruptured domain B, offshore of Hokkaido, Japan, in the vicinity of the 1952 Tokachi-oki earthquake. The rupture appears to have extended from about 25 to 45 km depth range, with the rupture zone within the 1952 rupture zone [*Yamanaka and Kikuchi*,

2003]. The rupture appears to be concentrated within domain B, with possible extension into domain C.

[50] 28 *March* 2005 *Sumatra* (M_w 8.6, m_b 7.0): The 2005 event ruptured the portion of the trench along Sumatra adjacent to the great 2004 event. The rupture occurred primarily in the central portion of the megathrust, as resolved by seismic and geodetic observations [*Ammon et al.*, 2005; *Walker et al.*, 2005; *Briggs et al.*, 2006; *Konca et al.*, 2007]. It was followed by significant afterslip on the shallower portions of the fault [*Hsu et al.*, 2006]. It appears to have ruptured domain B, and may have penetrated into domain C, with short-period radiation concentrating downdip of the regions of large slip imaged by broadband seismic and geodetic data (Figure A1).

[51] 16 *August* 2005 *Miyagi* (M_w 7.2, m_b 6.4): This is a moderate size event offshore of the Honshu coastline in the downdip region of the 11 March 2011 Tohoku earthquake that ruptured with strong short-period radiation. The rupture process documented by seismic wave and geodetic analyses [*Kanamori et al.*, 2006; *Miura et al.*, 2006] indicates that this event ruptured domain C.

[52] 17 *July* 2006 *Java* (M_w 7.8, m_b 6.0): This was a near-trench tsunami earthquake in the region along Java that does not have any documented great underthrusting events deeper on the megathrust. We rely on analysis of broadband seismic waves [*Ammon et al.*, 2006] for the characterization of this rupture as being in domain A. The largely extensional faulting aftershock activity [e.g., *El Hariri and Bilek*, 2011] is similar to that seen near the 1994 Java tsunami event and above the shallow large-slip region of the 2011 Tohoku rupture.

[53] 15 *November* 2006 *Kuril* (M_w 8.3, m_b 6.4): The central Kuril Islands region had uncertain seismogenic potential prior to the great earthquake doublet that struck on 15 November 2006 (M_w 8.3) and 13 January 2007 (M_w 8.1). The first event is a large shallow megathrust rupture and the second event is an outer trench-slope normal faulting event. Detailed analyses of body and surface waves [*Ammon et al.*, 2008; *Lay et al.*, 2009] along with some campaign GPS data [*Steblov et al.*, 2008] indicate that the slip zone for the 2006 event extended updip to the trench, rupturing domains A and B.

[54] 1 *April* 2007 *Solomon Islands* (M_w 8.1, m_b 6.7): The rupture for this event had slip concentrated at shallow depth with relatively low levels of short-period radiation [*Furlong et al.*, 2009; *Chen et al.*, 2009]. The event was tsunamigenic, but not as distinctively as typical tsunami earthquakes, even though it may have ruptured to the trench. The rupture appears to have initiated in domain B or the downdip region of domain A and ruptured updip and along-strike, crossing over a triple junction where two underthrusting plates enter the subduction zone.

[55] 15 *August* 2007 *Peru* (M_w 8.0, m_b 6.8): This event produced strong damage in Pisco, Peru and significant tsunami. It initiated near 40 km deep and ruptured updip, apparently as a composite event with about a 60 s delay between deeper and shallower subevents [*Lay et al.*, 2010a]. The primary slip appears to be in domain B, but the initial subevent is likely in domain C, with impulsive isolated rupture that triggered the shallower main event.

[56] 12 *September* 2007*a Sumatra* (M_w 8.4, m_b 6.6): This great earthquake rupture was located offshore of central Sumatra. The rupture does not appear to have extended to the trench [*Konca et al.*, 2008], although it abuts the downdip edge of the 25 October 2010 Mentawai rupture zone. Some slip may have occurred as deep as in the large aftershock on the same day (12 September 2007b), but the primary slip appears to be concentrated in domain B, with short-period radiation concentrated in the region of large slip (Figure A1).

[57] 12 *September* 2007*b Sumatra* (M_w 7.9, m_b 6.7): This earthquake ruptured the deeper portion of the megathrust below the region between the Pagai Islands and Sumatra (downdip of the 25 October 2010 Mentawai event). The event followed the larger thrust event to the southeast earlier on the same day. It generated relatively strong short-period radiation and failed in two large slip patches distributed along strike (Figure A1). E_r and E_r/M_o ratios were computed for the entire rupture process and the first subevent alone in Table 1 and Table 2. Body and surface wave analysis [*Konca et al.*, 2008] provides clear indication that this rupture was concentrated in domain C.

[58] 20 *February* 2008 *Sumatra* (M_w 7.4, m_b 6.5): This was a moderate size event that ruptured beneath Simeulue Island, Indonesia near the southern end of the 2004 Sumatra-Andaman rupture. The centroid depth and our own rupture model inversion indicate rupture in the depth range 15–30 km, placing this event in domain B.

[59] 29 *September* 2009 *Tonga* (M_w ~8): This underthrusting rupture was triggered by the 29 September 2009 trench-slope extensional-faulting earthquake south of Samoa, and ruptured from near the trench downdip over a width of about 50 km [*Lay et al.*, 2010c; *Beavan et al.*, 2010]. Weak short-period radiation from the rupture area is apparent in back-projections. Very few large thrust events occur in this region, so dynamic triggering of the event may have played a role in driving seismic failure of a conditionally stable portion of the shallow megathrust. We cannot determine a E_r/M_o ratio for the thrusting due to contamination of the signals by arrivals from the earlier normal faulting, but this rupture appears to have spanned domains A and B.

[60] 6 *April* 2010 *Sumatra* (M_w 7.8, m_b 6.8): This event occurred within the source region of the March 28, 2005 Nias earthquake, with slip concentrated in a patch between regions of large slip in the 2004 event. Finite fault modeling by NEIC and our own inversion indicates that it ruptured in the depth range 15–30 km, placing it in domain B.

[61] 25 *October* 2010 *Mentawai* (M_w 7.8, m_b 6.5): This earthquake ruptured the shallowest region of the megathrust off the Pagai Islands, Sumatra [*Lay et al.*, 2011b; *Bilek et al.*, 2011; *Newman et al.*, 2011]. The rupture appears to have spread updip from a hypocenter about 10 km deep on a very shallow dipping (7.5°) plane [*Singh et al.*, 2011]. The slow rupture process and concentration of slip near the toe of the trench, along with the strong tsunami that was generated are characteristic of tsunami earthquakes in domain A.

[62] **Acknowledgments.** This work made use of GMT and SAC software. Federation of Digital Seismic Networks (FDSN) seismic data were obtained from the Incorporated Research Institutions for Seismology (IRIS) Data Management System (DMS), and the F-net, K-net, Kik-net, and Hi-net data were obtained from National Research Institute for Earth Science and Disaster Prevention (NIED) data centers. We thank the Editor, Associate Editor, and two anonymous reviewers for their helpful comments on the manuscript. This work was supported by NSF grant EAR0635570 and USGS award 05HQGR0174.

References

Abercrombie, R. E., M. Antolik, K. Felzer, and G. Ekström (2001), The 1994 Java tsunami earthquake: Slip over a subducting seamount, *J. Geophys. Res.*, *106*, 6595–6607, doi:10.1029/2000JB900403.

Allmann, B. P., and P. M. Shearer (2009), Global variations of stress drop for moderate to large earthquakes, *J. Geophys. Res.*, *114*, B01310, doi:10.1029/2008JB005821.

Ammon, C. J., et al. (2005), Rupture process of the 2004 Sumatra-Andaman earthquake, *Science*, *308*, 1133–1139, doi:10.1126/science.1112260.

Ammon, C. J., H. Kanamori, T. Lay, and A. A. Velasco (2006), The 17 July 2006 Java tsunami earthquake, *Geophys. Res. Lett.*, *33*, L24308, doi:10.1029/2006GL028005.

Ammon, C. J., H. Kanamori, and T. Lay (2008), A great earthquake doublet and seismic stress transfer cycle in the central Kuril Islands, *Nature*, *451*, 561–565, doi:10.1038/nature06521.

Ammon, C. J., T. Lay, H. Kanamori, and M. Cleveland (2011), A rupture model of the 2011 off the Pacific coast of Tohoku earthquake, *Earth Planets Space*, *63*, 693–696, doi:10.5047/eps.2011.05.015.

Banerjee, P., F. Pollitz, B. Nagarajan, and R. Bürgmann (2007), Coseismic slip distributions of the 26 December 2004 Sumatra-Andaman and 28 March 2005 Nias earthquakes from GPS static offsets, *Bull. Seismol. Soc. Am.*, *97*, S86–S102, doi:10.1785/0120050609.

Beavan, J., X. Wang, C. Holden, K. Wilson, W. Power, G. Prasetya, M. Bevis, and R. Kautoke (2010), Near-simultaneous great earthquakes at Tongan megathrust and outer rise in September 2009, *Nature*, *466*, 959–963, doi:10.1038/nature09292.

Ben-Zion, Y. (2001), Dynamic ruptures in recent models of earthquake faults, *J. Mech. Phys. Solids*, *49*, 2209–2244, doi:10.1016/S0022-5096(01)00036-9.

Beroza, G. C., and S. Ide (2011), Slow earthquakes and nonvolcanic tremor, *Annu. Rev. Earth Planet. Sci.*, *39*, 271–296, doi:10.1146/annurev-earth-040809-152531.

Bilek, S. L. (2007), Using earthquake source durations along the Sumatra-Andaman subduction system to examine fault-zone variations, *Bull. Seismol. Soc. Am.*, *97*, S62–S70, doi:10.1785/0120050622.

Bilek, S. L., and E. R. Engdahl (2007), Rupture characterization and aftershock relocations for the 1994 and 2006 tsunami earthquakes in the Java subduction zone, *Geophys. Res. Lett.*, *34*, L20311, doi:10.1029/2007GL031357.

Bilek, S. L., and T. Lay (1998), Variation of interplate fault zone properties with depth in the Japan subduction zone, *Science*, *281*, 1175–1178, doi:10.1126/science.281.5380.1175.

Bilek, S. L., and T. Lay (1999), Rigidity variations with depth along interplate megathrust faults in subduction zones, *Nature*, *400*, 443–446, doi:10.1038/22739.

Bilek, S. L., and T. Lay (2002), Tsunami earthquakes possibly widespread manifestations of frictional conditional stability, *Geophys. Res. Lett.*, *29*(14), 1673, doi:10.1029/2002GL015215.

Bilek, S. L., E. R. Engdahl, H. R. DeShon, and M. El Hariri (2011), The 25 October 2010 Sumatra tsunami earthquake: Slip in a slow patch, *Geophys. Res. Lett.*, *38*, L14306, doi:10.1029/2011GL047864.

Briggs, R. W., et al. (2006), Deformation and slip along the Sunda megathrust in the great 2005 Nias-Simeulue earthquake, *Science*, *311*, 1897–1901, doi:10.1126/science.1122602.

Byrne, D. E., D. M. Davis, and L. R. Sykes (1988), Loci and maximum size of thrust earthquakes and the mechanics of the shallow region of subduction zones, *Tectonics*, *7*, 833–857, doi:10.1029/TC007i004p00833.

Chen, T., A. V. Newman, L. Feng, and H. M. Fritz (2009), Slip distribution from the 1 April 2007 Solomon Islands earthquake: A unique image of near-trench rupture, *Geophys. Res. Lett.*, *36*, L16307, doi:10.1029/2009GL039496.

Chlieh, M., et al. (2007), Coseismic slip and afterslip of the great M_w 9.15 Sumatra-Andaman earthquake of 2004, *Bull. Seismol. Soc. Am.*, *97*, S152–S173, doi:10.1785/0120050631.

Convers, J. A., and A. V. Newman (2011), Global evaluation of large earthquake energy from 1997 through mid-2010, *J. Geophys. Res.*, *116*, B08304, doi:10.1029/2010JB007928.

Delouis, B., J.-M. Nocquet, and M. Vallée (2010), Slip distribution of the February 27, 2010 Mw = 8.8 Maule earthquake, central Chile from static and high-rate GPS, InSAR, and broadband teleseismic data, *Geophys. Res. Lett.*, *37*, L17305, doi:10.1029/2010GL043899.

Dixon, T. H., and J. C. Moore (Eds.) (2007), *The Seismogenic Zone of Subduction Thrust Faults*, 680 pp., Columbia Univ. Press, New York.

Dziewonski, A. M., and D. L. Anderson (1981), Preliminary reference Earth model, *Phys. Earth Planet. Inter.*, *25*, 297–356, doi:10.1016/0031-9201(81)90046-7.

El Hariri, M., and S. L. Bilek (2011), Stress changes and aftershock distribution of the 1994 and 2006 Java subduction zone earthquake sequences, *J. Geophys. Res.*, *116*, B06306, doi:10.1029/2010JB008124.

Fujii, Y., and K. Satake (2007), Tsunami source of the 2004 Sumatra-Andaman earthquake inferred from tide gauge and satellite data, *Bull. Seismol. Soc. Am.*, *97*, S192–S207, doi:10.1785/0120050613.

Fujii, Y., K. Satake, S. Sakai, M. Shinohara, and T. Kanazawa (2011), Tsunami source of the 2011 off the Pacific coast of Tohoku earthquake, *Earth Planets Space*, *63*, 815–820, doi:10.5047/eps.2011.06.010.

Fukao, Y. (1979), Tsunami earthquakes and subduction processes near deep-sea trenches, *J. Geophys. Res.*, *84*, 2303–2314, doi:10.1029/JB084iB05p02303.

Furlong, K. P., T. Lay, and C. J. Ammon (2009), A great earthquake rupture across a rapidly evolving three-plate boundary, *Science*, *324*, 226–229, doi:10.1126/science.1167476.

Gudmundsson, Ó., and M. Sambridge (1998), A regionalized upper mantle (RUM) seismic model, *J. Geophys. Res.*, *103*, 7121–7136, doi:10.1029/97JB02488.

Hayes, G. P. (2011), Rapid source characterization of the 2011 M_w 9.0 off the Pacific coast of Tohoku earthquake, *Earth Planets Space*, *63*, 529–534, doi:10.5047/eps.2011.05.012.

Heaton, T. H. (1990), Evidence for and implications of self-healing pulses of slip in earthquake rupture, *Phys. Earth Planet. Inter.*, *64*, 1–20, doi:10.1016/0031-9201(90)90002-F.

Heuret, A., S. Lallemand, F. Funiciello, C. Piromallo, and C. Faccenna (2011), Physical characteristics of subduction interface type seismogenic zones revisited, *Geochem. Geophys. Geosyst.*, *12*, Q01004, doi:10.1029/2010GC003230.

Hsu, Y.-J., M. Simons, J.-P. Avouac, J. Galetzka, K. Sieh, M. Chlieh, D. Natawidjaja, L. Prawirodirdjo, and Y. Bock (2006), Frictional afterslip following the 2005 Nias-Simeulue earthquake, Sumatra, *Science*, *312*, 1921–1926, doi:10.1126/science.1126960.

Hu, Y., and K. Wang (2008), Coseismic strengthening of the shallow portion of the subduction fault and its effects on wedge taper, *J. Geophys. Res.*, *113*, B12411, doi:10.1029/2008JB005724.

Hyndman, R. D., and K. Wang (1993), Thermal constraints on the zone of major thrust earthquake failure: The Cascadia subduction zone, *J. Geophys. Res.*, *98*, 2039–2060, doi:10.1029/92JB02279.

Hyndman, R. D., K. Wang, and M. Yamano (1995), Thermal constraints on the seismogenic portion of the southwestern Japan subduction thrust, *J. Geophys. Res.*, *100*, 15,373–15,392, doi:10.1029/95JB00153.

Ide, S. (2012), Variety and spatial heterogeneity of tectonic tremor worldwide, *J. Geophys. Res.*, *117*, B03302, doi:10.1029/2011JB008840.

Ide, S., A. Baltay, and G. C. Beroza (2011), Shallow dynamic overshoot and energetic deep rupture in the 2011 M_w 9.0 Tohoku-Oki earthquake, *Science*, *332*, 1426–1429, doi:10.1126/science.1207020.

Iinuma, T., M. Ohzono, Y. Ohta, and S. Miura (2011), Coseismic slip distribution of the 2011 off the Pacific coast of Tohoku earthquake (*M* 9.0) estimated based on GPS data–Was the asperity in Miyagi-oki ruptured? *Earth Planets Space*, *63*, 643–648, doi:10.5047/eps.2011.06.013.

Imamura, F., N. Shuto, S. Ide, Y. Yoshida, and K. Abe (1993), Estimate of the tsunami source of the 1992 Nicaraguan earthquake from tsunami data, *Geophys. Res. Lett.*, *20*, 1515–1518, doi:10.1029/93GL01396.

Ishii, M. (2011), High-frequency rupture properties of the M_w 9.0 off the Pacific coast of Tohoku earthquake, *Earth Planets Space*, *63*, 609–614, doi:10.5047/eps.2011.07.009.

Ishii, M., P. M. Shearer, H. Houston, and J. E. Vidale (2005), Extent, duration and speed of the 2004 Sumatra-Andaman earthquake imaged by the Hi-Net array, *Nature*, *435*, 933–936, doi:10.1038/nature03675.

Ishii, M., P. M. Shearer, H. Houston, and J. E. Vidale (2007), Teleseismic *P* wave imaging of the 26 December 2004 Sumatra-Andaman and 28 March 2005 Sumatra earthquake ruptures using the Hi-net array, *J. Geophys. Res.*, *112*, B11307, doi:10.1029/2006JB004700.

Kanamori, H. (1972), Mechanism of tsunami earthquakes, *Phys. Earth Planet. Inter.*, *6*, 346–359, doi:10.1016/0031-9201(72)90058-1.

Kanamori, H. (1986), Rupture process of subduction-zone earthquakes, *Annu. Rev. Earth Planet. Sci.*, *14*, 293–322, doi:10.1146/annurev.ea.14.050186.001453.

Kanamori, H., and M. Kikuchi (1993), The 1992 Nicaragua earthquake: A slow tsunami earthquake associated with subducted sediments, *Nature*, *361*, 714–716, doi:10.1038/361714a0.

Kanamori, H., M. Miyazawa, and J. Mori (2006), Investigation of the earthquake sequence off Miyagi prefecture with historical seismograms, *Earth Planets Space*, *58*, 1533–1541.

Kanamori, H., L. Rivera, and W. H. K. Lee (2010), Historical seismograms for unravelling a mysterious earthquake: The 1907 Sumatra earthquake, *Geophys. J. Int.*, *183*, 358–374, doi:10.1111/j.1365-246X.2010.04731.x.

Kennett, B. L. N., E. R. Engdahl, and R. Buland (1995), Constraints on seismic velocities in the Earth from traveltimes, *Geophys. J. Int.*, *122*, 108–124, doi:10.1111/j.1365-246X.1995.tb03540.x.

Kikuchi, M., and Y. Fukao (1987), Inversion of long-period P-waves from great earthquakes along subduction zones, *Tectonophysics*, *144*, 231–247, doi:10.1016/0040-1951(87)90020-5.

Kiser, E., and M. Ishii (2011), The 2010 Mw 8.8 Chile earthquake: Triggering on multiple segments and frequency-dependent rupture behavior, *Geophys. Res. Lett.*, *38*, L07301, doi:10.1029/2011GL047140.

Koketsu, K., et al. (2011), A unified source model for the 2011 Tohoku earthquake, *Earth Planet. Sci. Lett.*, *310*, 480–487, doi:10.1016/j.epsl.2011.09.009.

Konca, A. O., V. Hjorleifsdottir, T.-R. A. Song, J.-P. Avouac, D. V. Helmberger, C. Ji, K. Sieh, R. Briggs, and A. Meltzner (2007), Rupture kinematics of the 2005 M_w 8.6 Nias-Simeulue earthquake from the joint inversion of seismic and geodetic data, *Bull. Seismol. Soc. Am.*, *97*, S307–S322, doi:10.1785/0120050632.

Konca, A. O., et al. (2008), Partial rupture of a locked patch of the Sumatra megathrust during the 2007 earthquake sequence, *Nature*, *456*, 631–635, doi:10.1038/nature07572.

Koper, K. D., A. R. Hutko, and T. Lay (2011a), Along-dip variation of teleseismic short-period radiation from the 11 March 2011 Tohoku earthquake (M_w 9.0), *Geophys. Res. Lett.*, *38*, L21309, doi:10.1029/2011GL049689.

Koper, K. D., A. R. Hutko, T. Lay, C. J. Ammon, and H. Kanamori (2011b), Frequency-dependent rupture process of the 2011 M_w 9.0 Tohoku earthquake: Comparison of short-period *P* wave backprojection images and broadband seismic rupture models, *Earth Planets Space*, *63*, 599–602, doi:10.5047/eps.2011.05.026.

Koper, K. D., A. R. Hutko, T. Lay, and O. Sufri (2012), Imaging short-period seismic radiation from the 27 February 2010 Chile (M_w 8.8) earthquake by backprojection of *P*, *PP*, and *PKIKP* waves, *J. Geophys. Res.*, *117*, B02308, doi:10.1029/2011JB008576.

Krüger, F., and M. Ohrnberger (2005a), Tracking the rupture of the M_w = 9.3 Sumatra earthquake over 1,150 km at teleseismic distance, *Nature*, *435*, 937–939, doi:10.1038/nature03696.

Krüger, F., and M. Ohrnberger (2005b), Spatio-temporal source characteristics of the 26 December 2004 Sumatra earthquake as imaged by teleseismic broadband arrays, *Geophys. Res. Lett.*, *32*, L24312, doi:10.1029/2005GL023939.

Kurahashi, S., and K. Irikura (2011), Source model for generating strong ground motions during the 2011 off the Pacific coast of Tohoku earthquake, *Earth Planets Space*, *63*, 571–576, doi:10.5047/eps.2011.06.044.

Lay, T., and S. Bilek (2007), Anomalous earthquake ruptures at shallow depths on subduction zone megathrusts, in *The Seismogenic Zone of Subduction Thrust Faults*, edited by T. H. Dixon and J. C. Moore, pp. 476–511, Columbia Univ. Press, New York.

Lay, T., H. Kanamori, C. J. Ammon, A. R. Hutko, K. Furlong, and L. Rivera (2009), The 2006–2007 Kuril Islands great earthquake sequence, *J. Geophys. Res.*, *114*, B11308, doi:10.1029/2008JB006280.

Lay, T., C. J. Ammon, A. R. Hutko, and H. Kanamori (2010a), Effects of kinematic constraints on teleseismic finite-source rupture inversions: Great Peruvian earthquakes of 23 June 2001 and 15 August 2007, *Bull. Seismol. Soc. Am.*, *100*, 969–994, doi:10.1785/0120090274.

Lay, T., C. J. Ammon, H. Kanamori, K. D. Koper, O. Sufri, and A. R. Hutko (2010b), Teleseismic inversion for rupture process of the 27 February 2010 Chile (M_w 8.8) earthquake, *Geophys. Res. Lett.*, *37*, L13301, doi:10.1029/2010GL043379.

Lay, T., C. J. Ammon, H. Kanamori, L. Rivera, K. D. Koper, and A. R. Hutko (2010c), The 2009 Samoa-Tonga great earthquake triggered doublet, *Nature*, *466*, 964–968, doi:10.1038/nature09214.

Lay, T., C. J. Ammon, H. Kanamori, L. Xue, and M. J. Kim (2011a), Possible large near-trench slip during the 2011 M_w 9.0 off the Pacific coast of Tohoku earthquake, *Earth Planets Space*, *63*, 687–692, doi:10.5047/eps.2011.05.033.

Lay, T., C. J. Ammon, H. Kanamori, Y. Yamazaki, K. F. Cheung, and A. R. Hutko (2011b), The 25 October 2010 Mentawai tsunami earthquake (M_w 7.8) and the tsunami hazard presented by shallow megathrust ruptures, *Geophys. Res. Lett.*, *38*, L06302, doi:10.1029/2010GL046552.

Lay, T., Y. Yamazaki, C. J. Ammon, K. F. Cheung, and H. Kanamori (2011c), The 2011 M_w 9.0 off the Pacific coast of Tohoku earthquake: Comparison of deep-water tsunami signals with finite-fault rupture model predictions, *Earth Planets Space*, *63*, 797–801, doi:10.5047/eps.2011.05.030.

Lorito, S., F. Romano, S. Atzori, X. Tong, A. Avallone, J. McCloskey, E. Boschi, and A. Piatanesi (2011), Limited overlap between the seismic gap and coseismic slip of the great 2010 Chile earthquake, *Nat. Geosci.*, *4*, 173–177, doi:10.1038/ngeo1073.

Maeda, T., T. Furumura, S. Sakai, and M. Shinohara (2011), Significant tsunami observed at ocean-bottom pressure gauges during the 2011 off the Pacific coast of Tohoku earthquake, *Earth Planets Space*, *63*, 803–808, doi:10.5047/eps.2011.06.005.

Marone, C., and C. H. Scholz (1988), The depth of seismic faulting and the upper transition from stable to unstable slip regimes, *Geophys. Res. Lett.*, *15*, 621–624, doi:10.1029/GL015i006p00621.

Meng, L., A. Inbal, and J.-P. Ampuero (2011), A window into the complexity of the dynamic rupture of the 2011 Mw 9 Tohoku-oki earthquake, *Geophys. Res. Lett.*, *38*, L00G07, doi:10.1029/2011GL048118.

Miura, S., T. Iinuma, S. Yui, N. Uchida, T. Sato, K. Tachibana, and A. Hasegawa (2006), Co- and post-seismic slip associated with the 2005 Miyagi-oki earthquake (M7.2) as inferred from GPS data, *Earth Planets Space*, *58*, 1567–1572.

Moore, G. F., N. L. Bangs, A. Taira, S. Kuramoto, E. Pangborn, and H. J. Tobin (2007), Three-dimensional splay fault geometry and implications for tsunami generation, *Science*, *318*, 1128–1131, doi:10.1126/science.1147195.

Moore, J. C., and D. Saffer (2001), Updip limit of the seismogenic zone beneath the accretionary prism of southwest Japan: An effect of diagenetic to low-grade metamorphic processes and increasing effective stress, *Geology*, *29*, 183–186, doi:10.1130/0091-7613(2001)029<0183:ULOTSZ>2.0.CO;2.

Newman, A. V., and E. A. Okal (1998), Teleseismic estimates of radiated seismic energy: The E/M_o discriminant for tsunami earthquakes, *J. Geophys. Res.*, *103*, 26,885–26,898, doi:10.1029/98JB02236.

Newman, A. V., G. Hayes, Y. Wei, and J. Convers (2011), The 25 October 2010 Mentawai tsunami earthquake, from real-time discriminants, finite-fault rupture, and tsunami excitation, *Geophys. Res. Lett.*, *38*, L05302, doi:10.1029/2010GL046498.

Ozawa, S., T. Nishimura, H. Suito, T. Kobayashi, M. Tobita, and T. Imakiire (2011), Coseismic and postseismic slip of the 2011 magnitude-9 Tohoku-Oki earthquake, *Nature*, *475*, 373–376, doi:10.1038/nature10227.

Peng, Z., and J. Gomberg (2010), An integrated perspective of the continuum between earthquakes and slow-slip phenomena, *Nat. Geosci.*, *3*, 599–607, doi:10.1038/ngeo940.

Poisson, B., C. Oliveros, and R. Pedreros (2011), Is there a best source model of the Sumatra 2004 earthquake for simulating the consecutive tsunami?, *Geophys. J. Int.*, *185*, 1365–1378, doi:10.1111/j.1365-246X.2011.05009.x.

Polet, J., and H. Kanamori (2000), Shallow subduction zone earthquakes and their tsunamigenic potential, *Geophys. J. Int.*, *142*, 684–702, doi:10.1046/j.1365-246x.2000.00205.x.

Pollitz, F., R. Bürgmann, and P. Banerjee (2011a), Geodetic slip model of the 2011 M9.0 Tohoku earthquake, *Geophys. Res. Lett.*, *38*, L00G08, doi:10.1029/2011GL048632.

Pollitz, F. F., et al. (2011b), Coseismic slip distribution of the February 27, 2010 Mw 8.8 Maule, Chile earthquake, *Geophys. Res. Lett.*, *38*, L09309, doi:10.1029/2011GL047065.

Rhie, J., D. Dreger, R. Bürgmann, and B. Romanowicz (2007), Slip of the 2004 Sumatra-Andaman earthquake from joint inversion of long-period global seismic waveforms and GPS static offsets, *Bull. Seismol. Soc. Am.*, *97*(1A), S115–S127, doi:10.1785/0120050620.

Rivera, L., and H. Kanamori (2005), Representations of the radiated energy in earthquakes, *Geophys. J. Int.*, *162*, 148–155, doi:10.1111/j.1365-246X.2005.02648.x.

Rushing, T., and T. Lay (2011), Analysis of seismic magnitude differentials (mb-Mw) across the megathrust faults in the vicinity of recent great earthquakes in Japan, Chile and Sumatra, Abstract U53D-0092 presented at 2011 Fall Meeting, AGU, San Francisco, Calif., 5–9 Dec.

Satake, K. (1994), Mechanism of the 1992 Nicaragua tsunami earthquake, *Geophys. Res. Lett.*, *21*, 2519–2522, doi:10.1029/94GL02338.

Scholz, C. H. (1998), Earthquakes and friction laws, *Nature*, *391*, 37–42, doi:10.1038/34097.

Seno, T., K. Shimazaki, P. Somerville, K. Sudo, and T. Eguchi (1980), Rupture process of the Miyagi-Oki, Japan, earthquake of June 12, 1978, *Phys. Earth Planet. Inter.*, *23*, 39–61, doi:10.1016/0031-9201(80)90081-3.

Shao, G., X. Li, C. Ji, and T. Maeda (2011), Focal mechanism and slip history of the 2011 M_w 9.1 off the Pacific coast of Tohoku earthquake, constrained with teleseismic body and surface waves, *Earth Planets Space*, *63*, 559–564, doi:10.5047/eps.2011.06.028.

Shimamura, K., T. Matsuzawa, T. Okada, N. Uchida, T. Kono, and A. Hasegawa (2011), Similarities and differences in the rupture process of the $M \sim 4.8$ repeating-earthquake sequence off Kamaishi, northeast Japan: Comparison between the 2001 and 2008 events, *Bull. Seismol. Soc. Am.*, *101*(5), 2355–2368, doi:10.1785/0120100295.

Simons, M., et al. (2011), The 2011 magnitude 9.0 Tohoku-Oki earthquake: Mosaicking the megathrust from seconds to centuries, *Science*, *332*, 1421–1425, doi:10.1126/science.1206731.

Singh, S. C., N. Hanamoto, M. Mukti, H. Permana, Y. Djajadihardja, and H. Harjono (2011), Seismic images of the megathrust rupture during the 25th October 2010 Pagai earthquake, SW Sumatra: Frontal rupture

and large tsunami, *Geophys. Res. Lett.*, *38*, L16313, doi:10.1029/2011GL048935.
Steblov, G. M., M. G. Kogan, B. V. Levin, N. F. Vasilenko, A. S. Prytkov, and D. I. Frolov (2008), Spatially linked asperities of the 2006–2007 great Kuril earthquakes revealed by GPS, *Geophys. Res. Lett.*, *35*, L22306, doi:10.1029/2008GL035572.
Suzuki, K., R. Hino, Y. Ito, S. Suzuki, D. Inazu, T. Iinuma, H. Fujimoto, M. Shinohara, and Y. Kaneda (2012), Seismicity near hypocenter of the 2011 off the Pacific coast of Tohoku earthquake deduced by using Ocean Bottom Seismographic data, *Earth Planets Space*, in press.
Tanioka, Y., and L. J. Ruff (1997), Source time functions, *Seismol. Res. Lett.*, *68*, 386–400, doi:10.1785/gssrl.68.3.386.
Tanioka, Y., and K. Sataka (1996), Fault parameters of the 1896 Sanriku tsunami earthquake estimated from tsunami numerical modeling, *Geophys. Res. Lett.*, *23*, 1549–1552, doi:10.1029/96GL01479.
Thatcher, W. (1989), Earthquake recurrence and risk assessment in circum-Pacific seismic gaps, *Nature*, *341*, 432–434, doi:10.1038/341432a0.
Tichelaar, B. W., and L. J. Ruff (1993), Depth of seismic coupling along subduction zones, *J. Geophys. Res.*, *98*, 2017–2037, doi:10.1029/92JB02045.
Tong, X., et al. (2010), The 2010 Maule, Chile earthquake: Downdip rupture limit revealed by space geodesy, *Geophys. Res. Lett.*, *37*, L24311, doi:10.1029/2010GL045805.
Uchida, N., and T. Matsuzawa (2011), Coupling coefficient, hierarchical structure, and earthquake cycle for the source area of the 2011 off the Pacific coast of Tohoku earthquake inferred from small repeating earthquake data, *Earth Planets Space*, *63*, 675–679, doi:10.5047/eps.2011.07.006.
Utsu, T. (2002), Relationships between magnitude scales, in *International Handbook of Earthquake and Engineering Seismology, Part A*, *Int. Geophys.*, vol. 81A, edited by W. H. K. Lee et al., pp. 733–746, Elsevier, London, doi:10.1016/S0074-6142(02)80247-9.
VanDecar, J. C., and R. S. Crosson (1990), Determination of teleseismic relative phase arrival times using multi-channel cross-correlation and least squares, *Bull. Seismol. Soc. Am.*, *80*, 150–169.
Velasco, A. A., C. J. Ammon, T. Lay, and J. Zhang (1994), Imaging a slow bilateral rupture with broadband seismic waves: The September 2, 1992 Nicaraguan tsunami earthquake, *Geophys. Res. Lett.*, *21*, 2629–2632, doi:10.1029/94GL02402.
Venkataraman, A., and H. Kanamori (2004), Observational constraints on the fracture energy of subduction zone earthquakes, *J. Geophys. Res.*, *109*, B05302, doi:10.1029/2003JB002549.
Vidale, J. E., and H. Houston (2012), Slow slip: A new kind of earthquake, *Phys. Today*, *65*, 38–43, doi:10.1063/PT.3.1399.
Vigny, C., et al. (2005), Insight into the 2004 Sumatra-Andaman earthquake from GPS measurements in Southeast Asia, *Nature*, *436*, 201–206, doi:10.1038/nature03937.
Vigny, C., et al. (2011), The 2010 M_w 8.8 Maule megathrust earthquake of central Chile, monitored by GPS, *Science*, *332*, 1417–1421, doi:10.1126/science.1204132.
Walker, K. T., M. Ishii, and P. M. Shearer (2005), Rupture details of the 28 March 2005 Sumatra M*w* 8.6 earthquake imaged with teleseismic P waves, *Geophys. Res. Lett.*, *32*, L24303, doi:10.1029/2005GL024395.
Wang, D., and J. Mori (2011a), Rupture process of the 2011 off the Pacific coast of Tohoku earthquake (M_w 9.0) as imaged with back-projection of teleseismic *P*-waves, *Earth Planets Space*, *63*, 603–607, doi:10.5047/eps.2011.05.029.
Wang, D., and J. Mori (2011b), Frequency-dependent energy radiation and fault coupling for the 2010 Mw8.8 Maule, Chile, and 2011 Mw9.0 Tohoku, Japan, earthquakes, *Geophys. Res. Lett.*, *38*, L22308, doi:10.1029/2011GL049652.
Wang, K., and J. He (2008), Effects of frictional behavior and geometry of subduction fault on coseismic seafloor deformation, *Bull. Seismol. Soc. Am.*, *98*, 571–579, doi:10.1785/0120070097.
Wang, K., and Y. Hu (2006), Accretionary prisms in subduction earthquake cycles: The theory of dynamic Coulomb wedge, *J. Geophys. Res.*, *111*, B06410, doi:10.1029/2005JB004094.
Xu, Y., K. D. Koper, O. Sufri, L. Zhu, and A. R. Hutko (2009), Rupture imaging of the M_w 7.9 12 May 2008 Wenchuan earthquake from back projection of teleseismic *P* waves, *Geochem. Geophys. Geosyst.*, *10*, Q04006, doi:10.1029/2008GC002335.
Yamanaka, Y., and M. Kikuchi (2003), Source process of the recurrent Tokachi-oki earthquake on September 26, 2003, inferred from teleseismic body waves, *Earth Planets Space*, *55*, e21–e24.
Yamanaka, Y., and M. Kikuchi (2004), Asperity map along the subduction zone in northeastern Japan inferred from regional seismic data, *J. Geophys. Res.*, *109*, B07307, doi:10.1029/2003JB002683.
Yao, H., P. Gerstoft, P. M. Shearer, and C. Mecklenbräuker (2011), Compressive sensing of the Tohuku-Oki Mw 9.0 earthquake: Frequency-dependent rupture modes, *Geophys. Res. Lett.*, *38*, L20310, doi:10.1029/2011GL049223.
Ye, L., T. Lay, and H. Kanamori (2012), The Sanriku-Oki low-seismicity region on the northern margin of the great 2011 Tohoku-Oki earthquake rupture, *J. Geophys. Res.*, *117*, B02305, doi:10.1029/2011JB008847.
Yomogida, K., K. Yoshizawa, J. Koyama, and M. Tsuzuki (2011), Along-dip segmentation of the 2011 off the Pacific coast of Tohoku earthquake and comparison with other megathrust earthquakes, *Earth Planets Space*, *63*, 697–701, doi:10.5047/eps.2011.06.003.
Yoshida, Y., H. Ueno, D. Muto, and S. Aoki (2011), Source process of the 2011 off the Pacific coast of Tohoku earthquake with the combination of teleseismic and strong motion data, *Earth Planets Space*, *63*, 565–569, doi:10.5047/eps.2011.05.011.
Yue, H., and T. Lay (2011), Inversion of high-rate (1 sps) GPS data for rupture process of the 11 March 2011 Tohoku earthquake (M_w 9.1), *Geophys. Res. Lett.*, *38*, L00G09, doi:10.1029/2011GL048700.
Zhang, H., Z. Ge, and L. Ding (2011), Three sub-events composing the 2011 off the Pacific coast of Tohoku Earthquake (M_w 9.0) inferred from rupture imaging by back-projecting teleseismic *P* waves, *Earth Planets Space*, *63*, 595–598, doi:10.5047/eps.2011.06.021.
Zhao, D., Z. Huang, N. Umino, A. Hasegawa, and H. Kanamori (2011), Structural heterogeneity in the megathrust zone and mechanism of the 2011 Tohoku-oki earthquake (Mw 9.0), *Geophys. Res. Lett.*, *38*, L17308, doi:10.1029/2011GL048408.
Zheng, G., and J. R. Rice (1998), Conditions under which velocity-weakening friction allows a self-healing versus a cracklike mode of rupture, *Bull. Seismol. Soc. Am.*, *88*, 1466–1483.

C. J. Ammon, Department of Geosciences, Pennsylvania State University, University Park, PA 16802, USA.
A. R. Hutko, Incorporated Research Institutions for Seismology Data Management Center, 1408 NE 45 St., Ste. 201, Seattle, WA 98105, USA.
H. Kanamori, Seismological Laboratory, California Institute of Technology, Pasadena, CA 91125, USA.
K. D. Koper, Department of Geology and Geophysics, University of Utah, Salt Lake City, UT 84112, USA.
T. Lay, T. M. Rushing, L. Ye, and H. Yue, Department of Earth and Planetary Sciences, University of California, Santa Cruz, CA 95064, USA. (tlay@ucsc.edu)